A ROBOTIC MANIPUALTOR FOR GRASPING AND LOCOMOTION

An Honors Thesis

Presented by

Brian Jin

Completion Date:
May 2016

Approved by:

_____

Frank C. Sup IV, Mechanical and Industrial Engineering

_____

Ian R. Grosse, Mechanical and Industrial Engineering

ABSTRACT

Title: A Robotic Manipulator for Grasping and Locomotion
Author: Brian Jin
Thesis/Project Type: Thesis
Approved By: Frank C. Sup IV, Mechanical and Industrial Engineering
Approved By: Ian R. Grosse, Mechanical and Industrial Engineering

This thesis presents a mechatronic design for a robotic end effector that demonstrates grasping and can be used as a method for locomotion. Robotic manipulation and locomotion are typically approached as separate problems. However, a hybrid function hand-foot manipulator has significant advantages over two single purpose designs by reducing the energy costs associated with performing both tasks. The goal of this thesis is to develop and assess robotic hand morphology for both locomotion and grasping. A successful design for manipulation is achieved by demonstrating the basic grasps defined in this project to be cylindrical, sphere, pinch, and hook. Locomotion is defined by specific loading conditions during quadrupedal motion, which are knuckle walking, falling, and rising from a prone position. These functions are realized through a novel series elastic wrist with one flexible finger and a rigid finger structure. The design of the finger including the compliant finger pad is optimized using finite element analysis and verified through experimental data. Specifications for the manipulator design are derived from the requirements of the uBot-7 located in the Laboratory for Perceptual Robotics at the University of Massachusetts Amherst.

ABSTRACT

Title: A Robotic Manipulator for Grasping and Locomotion
Author: Brian Jin
Thesis/Project Type: Thesis
Approved By: Frank C. Sup IV, Mechanical and Industrial Engineering
Approved By: Ian R. Grosse, Mechanical and Industrial Engineering

This thesis presents a mechatronic design for a robotic end effector that demonstrates grasping and can be used as a method for locomotion. Robotic manipulation and locomotion are typically approached as separate problems. However, a hybrid function hand-foot manipulator has significant advantages over two single purpose designs by reducing the energy costs associated with performing both tasks. The goal of this thesis is to develop and assess robotic hand morphology for both locomotion and grasping. A successful design for manipulation is achieved by demonstrating the basic grasps defined in this project to be cylindrical, sphere, pinch, and hook. Locomotion is defined by specific loading conditions during quadrupedal motion, which are knuckle walking, falling, and rising from a prone position. These functions are realized through a novel series elastic wrist with one flexible finger and a rigid finger structure. The design of the finger including the compliant finger pad is optimized using finite element analysis and verified through experimental data. Specifications for the manipulator design are derived from the requirements of the uBot-7 located in the Laboratory for Perceptual Robotics at the University of Massachusetts Amherst.

Table of Contents

Table of Figures

I. Introduction

A. Research Motivation

Effective methods of manipulation and locomotion represent some of the greatest challenges in the field of robotics today. However, to date the design of robotic manipulators and methods for locomotion are researched as separate entities. There has been no prior work on the development of a hybrid hand-foot design, which incorporates mechanisms for both grasping and locomotion. Such manipulators have the potential to extend the capabilities of legged robots and reduce the redundancy of leg and arm manipulators. As a benefit, the size and cost of the robot is reduced. The dual function of the hand requires the ability to survive loading experienced during locomotion as well as the extreme case of impact loads when balance is lost. These mechanisms provide support in grasping and locomotion activities, reducing the difficulty of the tasks and the energy costs associated with locomotion. Furthermore, this type of manipulator design has significant impacts in the general field of robotics, allowing for a model with dexterous grasping capabilities and the ability to survive collisions with objects and the environment.

A more concrete application of this research is demonstrated through Honda's new ASIMO robot designed for disaster response missions. In extreme environments where the terrain is both unpredictable and hazardous, robust structural designs are critical for disaster response robots to prevent damage during operation. Honda's new ASIMO is envisioned to posses the capability to transition from bipedal motion to quadrupedal motion. This ability requires a durable robotic hand that can support the weight of the robot in addition to surviving rough environments that robot must explore. Most robotic manipulators under research are focused on improving dexterity, but few are designed with the intent to support body weight. The

research conducted in this honors thesis focuses on the design of a robust robotic manipulator that can be used in quadrupedal motion.

B. Research Objective

The goal of this thesis is to formalize the design of a dual function manipulator prototype for grasping and locomotion and then build a prototype of the design for experimental validation. The manipulator will demonstrate the basic grasps defined in this project to be cylindrical grasp, hook grasp, and pinch grasp. The cylindrical grasp can also be applied to spherical objects. For locomotion, the design will leverage two-finger gripper morphology to improve the prototype's resistance to external loading damage. Additionally, the end effector will incorporate a series elastic actuated wrist to protect the actuator from damage during quadrupedal motion. The wrist mechanism must also demonstrate a 20 degree flexion and 45 degree extension, the approximate range of motion for a human wrist. The end effector will be designed specifically for the uBot-7, which is located in the Laboratory of Perceptual Robotics at the University of Massachusetts Amherst.

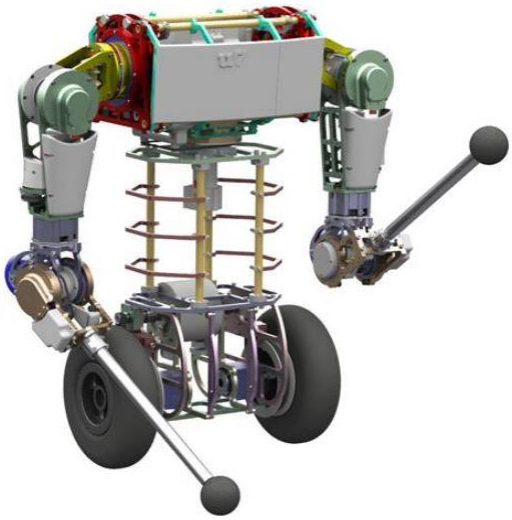

Figure 1 - Computer rendition of the uBot-7

Based on the design goals, the manipulator must sustain an impact load of 30 kg, roughly the weight of the uBot-7, dropped from a 0.5 meter height. Given the purpose of the uBot-7 is to function as a service robot, the initial prototype must demonstrate the ability to grasp common household objects defined later in this paper. The prototype must also demonstrate grasps of common objects defined later in this paper. Additionally, the design goal of the prototype is to weigh less than 1.0 kg to demonstrate the practical implementation of a hybrid hand-foot manipulator onto a robot.

C. Research Scope and Approach

This thesis is organized into three sections. The first section is to identify and detail a morphology for the grasping mechanism. The second section is to implement a wrist mechanism and series elastic actuation to the manipulator for improving locomotion capabilities. The third section is to develop system architecture and a basic controller for the manipulator. The third section extends beyond the scope of this thesis, but a framework for the controller will be presented for future work.

II. Background

A plethora of literature has been published within the last decade dealing with robotic hand designs for manipulation and grasping. The review of the literature will present successful mechanical, sensory, and control design approaches for robotic hands with grasping capabilities that can be implemented and experimentally validated.

1) Manipulation and Grasping

Research in robotic manipulators can be grouped into two categories: hands designed primarily for manipulating objects and hands for grasping objects [1]. Manipulating objects in free space requires arbitrarily positioning and orienting the object with respect to the base of the hand while maintaining a stable grip on the object. Object manipulation requires high dexterity, advanced sensors, and complex control algorithms. Robotic hands that achieve this functionality often suffer from complex and expensive designs as well as a reduced payload. Grasping tasks are less complex than manipulation tasks and are relevant in many industrial applications. While the simple grippers can achieve a gripping motion, they are often impractical because they can not adapt to arbitrarily shaped objects. In both areas, studies are focused on the design and mathematical modeling of these manipulators. Salisbury performed work modeling the closure properties of grasps with different contacts [2].

Rodriguez et al. looked at grasping from a different approach by studying the relationship between caging and grasping an object [3]. The definition of caging an object is to limit the mobility of the object. While the caged object maintains a certain degree of movement, the position of the object can still be manipulated in free space by moving the cage. Caging contrasts the prehensile approach to object manipulation, which requires movement to be restricted

completely. Most manipulators desire full control over an object and therefore the object must be immobile. Rodriguez et al. introduce the concept of a pre-grasping cage, which is a caging configuration that can be adjusted for a complete grasp of an object without breaking the cage. They show that for all two-fingered manipulators, all cages are pre-grasping cages, leading to a useful geometry for grasping objects. For cages created by manipulators with greater than two fingers, successful grasps using the cage as a waypoint is not always achievable.

A dexterous manipulator must achieve the functions of reaching and preshaping, grasping, manipulation with stable grasp, exploration with sensori-motor coordination, and gesture expressiveness [4]. Designers of the CyberHand describe the basic human hand capabilities to be reaching, grasping, exploring, manipulation, and gesture expression [5]. In terms of grasping capabilities, many papers have similar definitions for the fundamental grasping capabilities of a hand. Professors from the Universiti Teknologi MARA in Malaysia define grasping capabilities to be cylindrical, tip, hook or snap, palmer, spherical and lateral or key pinch grasp [6]. Other researchers have described the basic grasping functions to be cylindrical grasp, precision grasp, hook prehension, tip grasp, spherical grasp, and lateral hip [7]. Given the minimal variation in grasping definitions between research papers, the major grasping capabilities of an effective hand can be summarized into six basic functions, which are cylindrical, precision, hook, spherical, lateral, and tip.

2) Morphology for Manipulation and Grasping

The most common approach for designing robotic hands is an anthropomorphic design approach. Anthropomorphic designs attempt to mimic the characteristics of the human hand. Many researchers implement anthropomorphic designs because the high functionality of the

human hand represents the benchmark for achieving the perfect design. The anthropomorphic design imitates fundamental structures of human hand (weight, dimensions, number of fingers, degrees of freedom, finger kinematics, etc.) and its essential functions. In general, dimensions of the body and fingers are modeled closely to the physical characteristics of the human hand.

While anthropomorphic designs are not ubiquitous among robotic hands, the majority of morphology for dexterous manipulators is derivative of the anatomy of the human hand. The finger can be organized into two different categories, the normal finger and the thumb. The normal finger is composed of three phalanges and one bone; they are the distal phalange (DP), the middle phalange (MP), the proximal phalange (PP), and the metacarpal bone (MB). Each phalange is connected by three joints, which are the distal interphalangeal joint (DIP), the proximal interphalangeal joint (PIP), and the metacarpo phalangeal joint (MCP) [7]. The average range of motion for flexion and extension is 65 degrees for the DIP, 100 degrees for the PIP, and 80 degrees for the MCP. Abduction and adduction angles for the index finger are about 20 degrees at the MCP [6]. The thumb only has two phalanges and one bone, which are the DP, the PP, and the MB respectively. The joints of the thumb are the interphalangeal joint, the MCP, and the trapeziometacarpal joint, which has two degrees of freedom. Flexion and extension of the finger is performed by the contraction of specific muscles. These muscles are connected to the bones via specific tendons. The flexor digitorum superficialis tendon is fixed to the bottom of the middle phalange and it is used for the flexion of the proximal phalange and the middle phalange. The flexor digitorum profundus tendon is fixed to the bottom of the distal phalange, and it is used for the flexion of the DP and the MP [7].

Given the anatomy of the human hand, certain combinations of finger postures are impossible to achieve for most people. In terms of biomechanics, this means that the human hand

is equivalent to an underactuated system. An underactuated system is a system where the number of effective actuators in the system is less than the number of degrees of freedom. In mathematical terms, this means that the size of the input vectors for controlling the hand has a smaller dimension than the size of the output state vectors [5]. Fortunately, the natural equivalence of a human hand to an underactuated system is advantageous from a design perspective. The reduction of the number of actuators to operate the same number of degrees of freedom simplifies the design and reduces the weight. Underactuated systems also distribute torque more evenly throughout the system and allow for adaptive grasps [5]. All of the robotic hand designs reviewed implement some method of underactuation. The most common example of underactuation involved using a single actuator to transmit motion to the DIP, PIP, and MCP joints of each finger.

The typical robotic hand has either three fingers or five fingers to manipulate objects. Three-finger designs, such as the tendon-driven three finger robotic hand, are studied because they are considered the minimum number of fingers necessary to perform basic desired grasping tasks [7]. In addition, they tend to be lighter and less expensive. Five-finger robotic hands, such as the DLR/HIT Hand II, are designed to have a greater resemblance to the human hand with the tradeoff of increasing the weight and price.

In the context of locomotion, there is little discussion on the types of loads that the robotic hands can handle. Instead, the design focus is primarily achieving dexterous manipulation through different mechanisms and control. Consequently, the largest discussion revolves around the mechanisms behind operating the fingers and thumb. The hand design proposed by engineers at the Dong-Eui University in Pusan, Korea is a tendon driven three-finger design where each finger flexion is driven by a single DC motor [7].

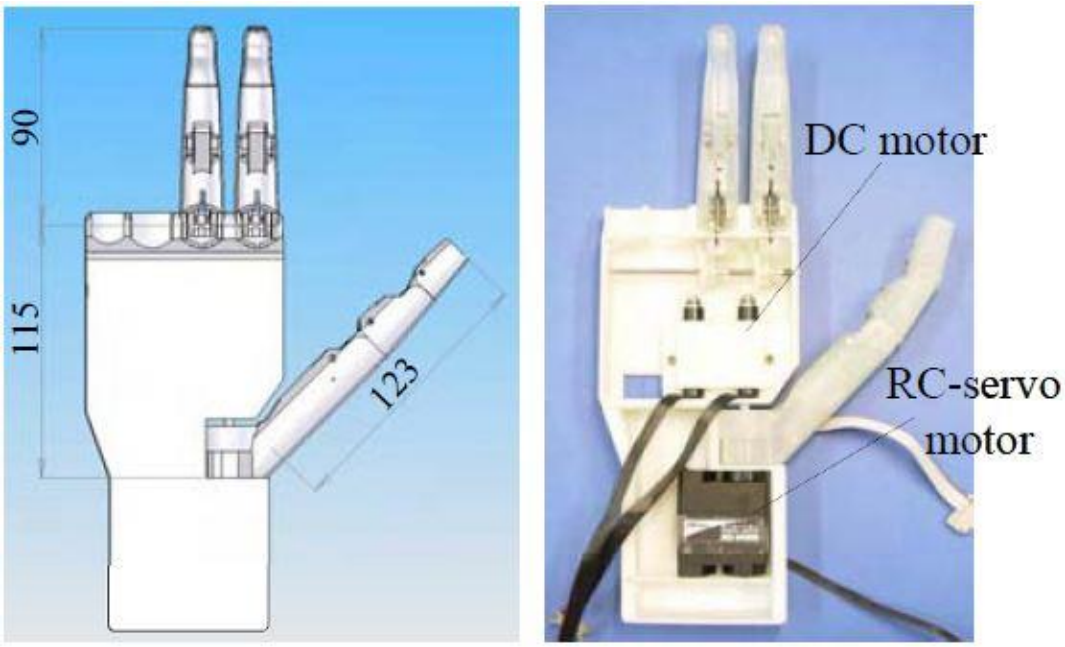

Figure 2 – Left: dimensions of the three-finger design (mm), Right: actuators used for the hand

In order to reduce the number of actuators, they introduce three design concepts. The first concept combines the DP and MP into a single phalange structure as opposed to two separate components. The second concept introduces a link mechanism between the MCP and PIP of the thumb. The third concept adopts a restoration spring to mimic the extension muscles of the human finger. Bearings are used to minimize joint friction and a combination of a cable-pulley system and a link system is implemented to transfer the motor actuation [7]. Each finger is actuated by a single DC motor; meanwhile the thumb is actuated by two motors due to the trapeziometacarpal joint. Given the shape of the hand and its material composition, which is mostly plastic, the hand is unsuitable for locomotion activities. In the paper, no discussion is made on the types of loads that the hand can sustain.

Researchers from the Campus Biomedico University and the Advanced Robotics Technology and Systems Laboratory in Italy present a three-finger mechanical design similar to the tendon drive three-finger design where the index, middle and thumb each were driven by one

DC motor. Each finger has a cable that runs along the volar side and wrapped around idle pulleys placed at each joint. Extension of the finger is achieved by torsion springs placed at each joint as opposed to a linear spring that is placed in the tendon drive three-finger design [8]. Similar to the previous three-finger design, this device was not designed to sustain any particular loads associated with locomotion, and there is no indication that the morphology can be adapted to perform locomotion tasks.

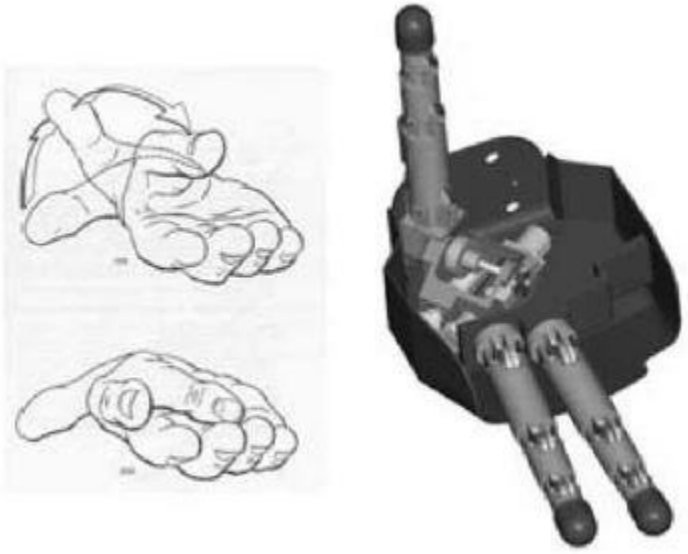

Figure 3 – Illustration of the Campus Biomedico Hand

The fingers of the RL1 hand, designed by engineers at the Universidad Carlos II de Madrid, also operate in a similar cable-pulley system as the other two hands discussed above. The hand is designed for the ASIBOT robot, which is an assistive robot designed for domestic environments. Although the structure of the hand is not anthropomorphic, the physical characteristic and kinematic design of the fingers is modeled off human fingers. The unique aspect of the design behind the RL1 Hand is that the engineers focused on optimizing the placement of the primary and secondary pulleys to increase the efficiency of the generated

moment by 36.5% [9]. This optimization method exploits the most strength out of the tendon cable and results in a steady and more precise grasp of the various tested objects.

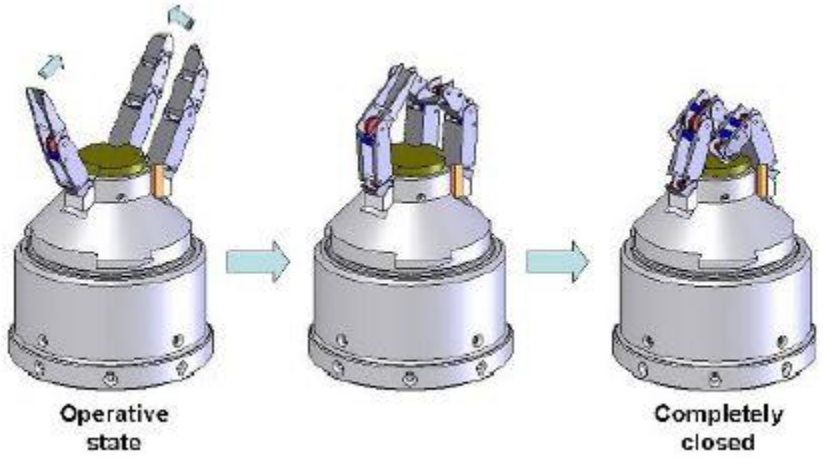

Figure 4 - RL1 Hand finger actuation

The design of the RL1 hand is unique because the fingers can retract into the arm and remain fully encapsulated. This feature was implemented to protect the fingers while reducing the profile of the hand during its inactive period. With the ability to protect the fragile components of the hand, the morphology of the RL1 hand can be adapted to sustain dynamic loads associated with locomotion.

The three robotic hands discussed above introduce a number of general design mechanisms that are common among most anthropomorphic robotic hands developed prior to the year 2005. The first similarity is the implementation of restoration springs for extension of the finger. The second similarity is the use of a cable-pulley system to perform flexion, mimicking the tendons and muscles of the human finger. The third similarity is the use of a single dc motor to actuate each finger and two dc motors to actuate the thumb, where DC motors are placed in the palm section of the hand. These three elements summarize the majority of the mechanical designs for anthropomorphic robotic hands that have been proposed in the early half of the last decade. The RL1 hand in particular stands out for its potential for locomotion. Recently, more

creative mechanical approaches towards optimizing the anthropomorphic robotic hand have been attempted and experimentally validated. Many of these new approaches focus on improving grasping power without sacrificing the size and weight of the hand. However, many of the hands continue to provide little information on their ability to support loads or potential to perform locomotion tasks.

One of the more modern robotic hands under study is the NAIST hand system developed by a collaboration of engineers from the Georgia Institute of Technology and the Nara Institute of Science and Technology (NAIST). The hand has a total of four fingers where each finger has three degrees of freedom. Two of the degrees of freedom are for the MCP and one degree of freedom is for the PIP. Similar to the three tendon hand design, the NAIST combines the DP with the PP to simplify movement.

Figure 5 - NAIST Hand

The unique design approach to the NAIST is that there is no cable-pulley system to mimic the tendons of the human hand. Cable-pulley systems are advantageous because the flexibility of the wires allow the actuators for the fingers to be placed outside of the hand, and they allow the implementation of larger actuators, which produce high force and speed [10]. While they are widely used in the design of many anthropomorphic hands, the cable-pulley

system is complex in nature, requiring advanced kinematics for dexterous control. As a result, having precise control over the fingers is difficult and regular maintenance of the cable-pulley system is necessary [10]. In addition, they are not reliable for long term use. Instead, a special three-axis gear driving mechanism is proposed that allows the placement of all three electrical motors that drive the finger joints to be located in the palm of the hand [11]. Finger joints are connected through rigid links as opposed to cables. Physically, the NAIST is too large and clunky to be adapted to a human body; however the hand has demonstrated applicability for serial manipulators and possible humanoid robots. The main achievement of the NAIST is the proof of concept design that a cable-pulley system may not be the optimal system for emulating the human hand. The design's metal composition shows that it has the ability to sustain higher loads in comparison to many of the previous reviewed designs. However, the morphology of the design is not practical for locomotion because the finger joints create a nonlinear contact relationship between the ground and the hand. Predictable contact behavior is desirable so that the robot will have better control over its movement.

A follow up to the NAIST Hand design produced the NAIST Hand 2, proposed by engineers at the Nara Institute of Science and Technology. The design of the NAIST Hand 2 focuses on improving the size and finger tip force of the previous design. In order to increase the finger tip force, engineers reintroduce the tendon driven model that the NAIST design originally rejected. The weaknesses of the cable-pulley system are addressed by locating the actuators outside of the body. This design is achieved by a gear mechanism attached at the wrist section of the hand. The mechanism consists of a series of gears placed on a single shaft that represents the wrist of the NAIST Hand 2. Locating all the gears on one shaft allows for simple correction of the mutual interference between the wrist and finger motions [10].

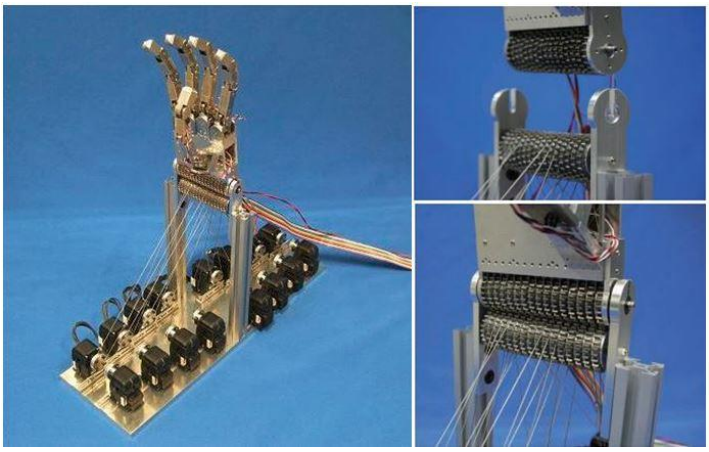

Figure 6 - NAIST Hand 2 with detachable wrist mechanism

The gear mechanism also allows the hand to detach from the actuators. The detachability of the actuators improves the ease of performing standard maintenance of the cable-pulley system, which theoretically improves the life expectancy and precision of the fingers. A special pulley design is also introduced to reduce the size of the fingers so that they have a stronger resemblance to the average human finger. This pulley consists of a cover and a base with a groove to guide the wire. This pulley is implemented at every joint of the finger. Similar to all the robotic hands previously discussed, the finger module itself is designed based on the anatomy of the human finger. Three segments of the finger represent the DP, MP, and PP of the human finger. The flexion and extension motions of the DIP joint are coupled with the PIP motions by a special link, which is a similar technique implemented in the tendon-driven three finger design previously discussed [7]. Compared to the size of the NAIST, the size of the NAIST Hand 2 is reduced significantly to dimensions within 5% of an adult male hand [10]. The finger tip force achieves scales according to the power of the actuator; however the actuators used for the NAIST Hand 2 prototype achieves only about 10 N of force. Regarding locomotion, the NAIST Hand 2 possesses the same advantages and disadvantages as the first iteration.

Another modern robotic hand design is proposed by engineers at the Korea Institute of Science and Technology. A typical anthropomorphic finger is operated by a rotary motor powering a combination of gear sets and pulleys. However studies of the human hand indicate the presence of certain coupled muscles that generate finger movements and not just the flexor digitorum superficialis tendon and the flexor digitorum profundus tendon in the finger [12]. As a result, the proposed robotic hand features four fingers, each driven by two linear actuators via a coupled link mechanism.

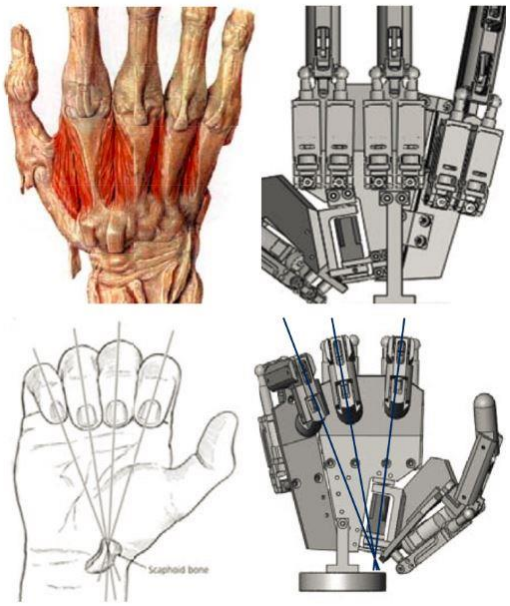

Figure 7 - Diagram of coupled muscles and linear actuators implemented to mimic those muscles

Linear actuators are selected instead of rotary actuators because linear actuators are lighter than rotary motors and typically produce more power. Additionally, the force, position, and speed of the linear actuators are more precise and easier to control [12]. The linear actuators are located below the knuckle section of the hand. In addition, compared to previously proposed finger designs, an extra degree of freedom is incorporated in the palm and thumb of the hand. The degree of freedom in the palm mimics the saddle joint of the human thumb. The extra degree of freedom allow for the thumb to mate oppositely with any finger on the hand. The result of this

unique biomemetic design is an efficient power transmission to the fingers compared to the typical hand designs. Similar to the NAIST hand, the proposed finger design does not incorporate a cable-pulley system for operating motion, but instead employs two simple links to transmit the actuator motion to each phalange [10]. The results of the unique approach is an anthropomorphic hand roughly 1.2 times the size of a normal hand with a grasp force that reaches approximately 30N of force [12]. Typical finger force requirements are only about 10N of force. Given the structure of the hand, the morphology can not be adapted for locomotion.

Another hand that incorporates a unique actuator is the DLR/HIT Hand II pictured below.

Figure 8 - DLR/HIT Hand II

This hand uses super flat brushless DC (BLDC) motors for actuation. As the name suggests, super flat BLDC motors are compact forms of regular dc motors. Super flat BLDC motors minimize the weight and size of the hand without sacrificing the same proportion of power [13]. In addition to the motors, the DLR/HIT Hand II replaces the gear and linkage transmission in the finger with timing belts and steel wire transmission, which increases flexibility and safety. The

timing belt and steel wire transmission is similar to the cable-pulley system except the timing belt and steel wire transmission coupled with a parallel flat BLDC motor configuration allows the entire system to operate more consistently and to have more flexible stiffness [13]. The shape of the DLR/HIT Hand II resembles closely to the human hand. There is potential for locomotion if the hand is clenched into a fist and is used for knuckle walking. However, there is no protection for the internal components of the hand.

A more unorthodox approach to the design of an anthropomorphic hand is a three-finger design proposed by a group of engineers from the Keio University in Japan. The proposed design uses electro-conjugate fluid to transmit motion to the fingers, as opposed to using any type of motor. Electro-conjugate fluid is a kind of dielectric fluid that produces a jet flow when it is subjected to a high DC voltage [14].

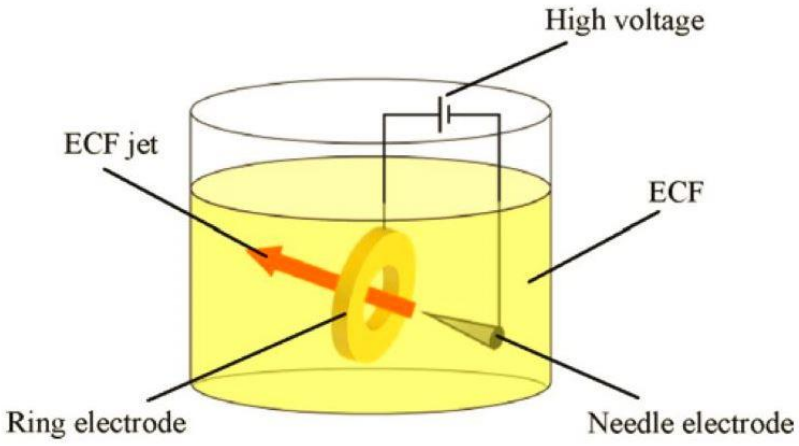

Figure 9 - Electro-conjugate fluid operation

The advantage of using electro-conjugate fluid (ECF) as a power source for actuation is that ECF increases in power as the electrode pairs used to induce the flow get closer together, which means that power increases as spacing decreases. This technology could potentially decrease the size of the robotic hand without sacrificing power. Grasping motion is achieved by increasing the pressure inside specially designed fingers. The fingers are constructed from flexible material

reinforced with special fibers that will cause the fingers to bend when pressurized [14]. While there are other robotic hands that operate using pneumatic pressure, the ECF hand differs from any other design because the working fluid is completely enclosed within the hand, and the actuator and pressure sources are integrated in the hand. Compared to previously discussed robotic hands which have rigid interactions with their environments, the ECF hand deals in the field of soft robotics and is highly compliant when dealing with other objects. Experimentally, the ECF hand is capable of grasping objects; however there are still a number of challenges to overcome before the technology can be implemented practically.

In summary, the robotic hands developed in the late half of the previous decade have demonstrated alternative approaches towards achieving the motion and grasping capabilities of the human hand. The NAIST Hand, dual linear actuator hand, DLR/HIT Hand II and ECF hand all deviate from the widely used cable-pulley system for finger operation and instead implement alternative methods. The NAIST Hand II returns to the cable-pulley transmission but attempts to locate the actuators outside of the hand to minimize the hand weight. The dual linear actuator hand, DLR/HIT Hand II, and NAIST Hand II all achieve weights and dimensions close to the human hand, although all are still slightly heavier and larger than the benchmark. The ECF hand is a revolutionary approach to the robot hand design; however the nascent technology is still behind the well established rigid mechanical systems regarding practical implementation onto a robot. Out of all the reviewed hands, none have addressed the potential to be used for locomotion. The morphology of the RL1 hand has the greatest potential to be adapted for locomotion, while the material composition of the NAIST hand provides the structural integrity for dynamic loads associated with locomotion.

3) Sensory and Control

Once the mechanical design of the robotic hand is achieved, the final step is to determine the hand's sensory system and the optimal control algorithm for finger motion. Sensory systems are essential for the operation of robot hands because they provide feedback information for the microprocessors to control the actuators. Control algorithms ensure that the fingers of the hand physically perform according to their intended input trajectories. Dexterous robotic hands require a minimum set of force and position sensors in order to implement successful control schemes, such as position control and impedance control [13]. A robotic hand can functionally perform closer to the abilities of a human hand when there are a greater number of sensors available for the controller.

Robotic hands in the late stages of development and testing have the most well developed sensory systems. The CyberHand, developed by Swedish and Italian engineers, has a complex sensory system that is organized into two subsystems: the proprioceptive subsystem and the exteroceptive subsystem [5]. The proprioceptive sensors provide information about hand position, movement, and internal forces. The exteroceptive sensors provide information about the interaction between the CyberHand and a particular object, as well as the interaction between the particular object and its environment. Proprioceptive sensors consist of joint angle sensors for position control, incremental magnetic encoders on each motor for finger position control, and tension sensors in cable transmission to monitor force applied by actuators. The exteroceptive sensors consist of a flexible layer that contains contact sensors to cover the hand, tri-axial force sensors integrated in the finger tips, and a compliant skin with embedded 3D force microsensors to measure the force distribution at the finger tips [5]. The modular approach of the design of the CyberHand requires that a sensory system has redundancies so that the hand is flexible and

allows for multiple implementations and comparisons of control strategies. When an object is in contact with the CyberHand, position control is switched to force control. Only force and contact sensors are used. For both the low level and high level control system, a proportional-integrator-derivative (PID) control model is used. High level control interprets the signals sent by the brain and estimates the desired grasp and relative forces applied. The information is then sent to the low level control. Two force errors, global grip force error and finger force error, are evaluated in the control loop. Results indicated that the simple control algorithm implemented was robust and required a minimal number of sensors. Slippage was not completely avoided due to long reaction time of the system, which was about 50ms. The entire hand had a stable grasp 96% of the time during trial period. Grasping was resilient and the hand recovered in less than .5 seconds from destabilizing loads. The experiments indicated that precision grasps are difficult to achieve due to mechanical characteristics of the hand and the stiffness of the fingers.

The DLR/HIT Hand II is on a similar level of development as the CyberHand. The DLR/HIT Hand II has an incredibly complex sensory architecture. Every joint is equipped with a strain gauge based torque sensor. The finger tips have a 6 degree of freedom sensor and a piezoresistive tactile sensor array is under development for even more accurate contact area measurements [13]. Every finger is also equipped with signal processing circuit boards. Similar to the Cyberhand, the DLR/HIT Hand II's intricate sensory system allows for a modular control system. The control system for the DLR/HIT Hand II is not described in the same detail as the CyberHand; however the vast array of sensors and embedded system design allow for a multitude of different control designs comparable to the CyberHand's control design.

For robotic hands still in the earlier stages of research, the bio-mimetic hand operated by coupled linear actuators has a less intricate sensory system than the CyberHand and the

DLR/HIT Hand II, but it does employ a film type tactile sensor at the finger tips and palm [12]. Unlike the control scheme implemented in the Cyberhand, the control scheme for the fingers is a proportional derivative (PD) hybrid position/force controller. The controller properly recognizes the distinction between force control and position control subspaces. The biomechatronic hand previously discussed above also incorporates a variation of the PD control model for the finger. This PD controller is applied in both the joint space and slider space, and it incorporates gravity compensation and elastic compensation for preloaded springs.

Even more basic control and sensory systems have been implemented in early models. The NAIST Hand II employs only a proportional controller with no compensation for gear backlash [10]. The multi-fingered anthropomorphic robotic hand proposed by A. Jaffar, Bahari, Low, and R. Jaafar, appears to use either open loop control or switch state logic, where a simple light sensor placed in the palm region triggers the grasping motion of the fingers [6]. The high performance anthropomorphic hand proposed by Takaki and Omata does not appear to employ a control algorithm; however its sensory system is unique compared to any of the other robotic hands reviewed [15]. Instead of installing separate sensors, the hand senses by measuring motor current. At a constant voltage supplied by a power supply, the current depends on the angular velocity of the finger joint. When the finger makes contact with the object, the angular velocity of the finger joint decreases as the current increases. Therefore, if the motor current exceeds a certain threshold in a given period of time, then the finger has made contact with the object.

III. Mechanical Design

A. Specifications and Design Process

Specifications for the design are derived from the requirements of the uBot-7, a service robot intended for helping around the house. A picture of the uBot-7 including critical dimensions is displayed in the figure below.

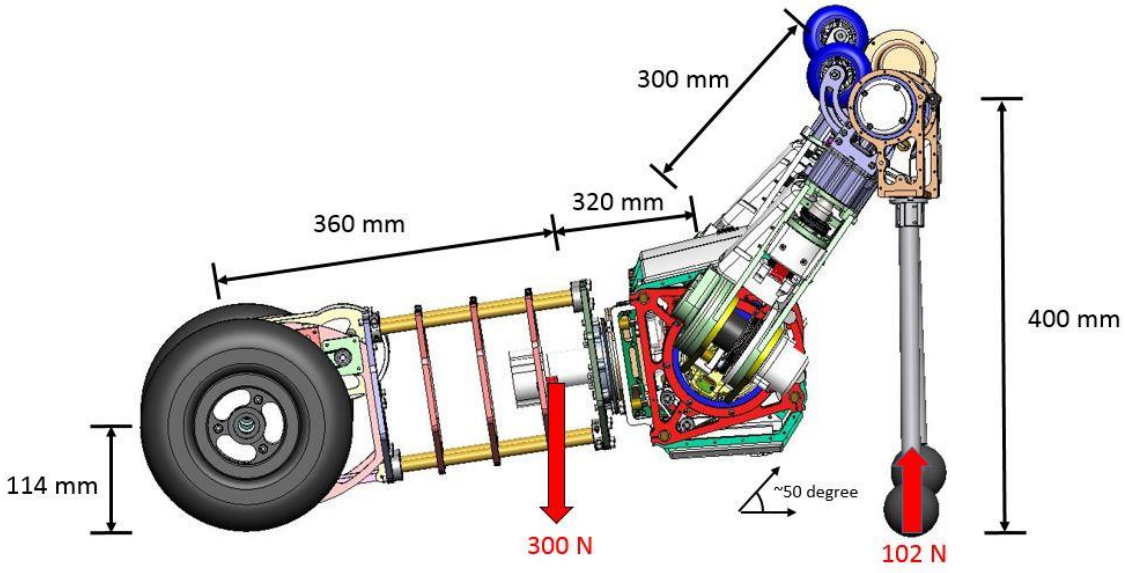

Figure 10 - Principle dimensions of the uBot-7, including loads

The current end effectors for the uBot-7 are rubber balls that allow the robot to perform quadrupedal locomotion and certain two points of contact grasps. The design solution must extend the grasping abilities of the uBot-7 while maintaining its ability to perform quadrupedal locomotion. One of the critical uses of the end effectors for the uBot-7 is to recover from a prone position. This function is necessary for any circumstance where the robot loses its balance and falls flat on its front or back. For this type of locomotion task, the manipulator must be versatile

so that the uBot-7 can return from a prone position by multiple means. Figure 11 below describes examples of these motions.

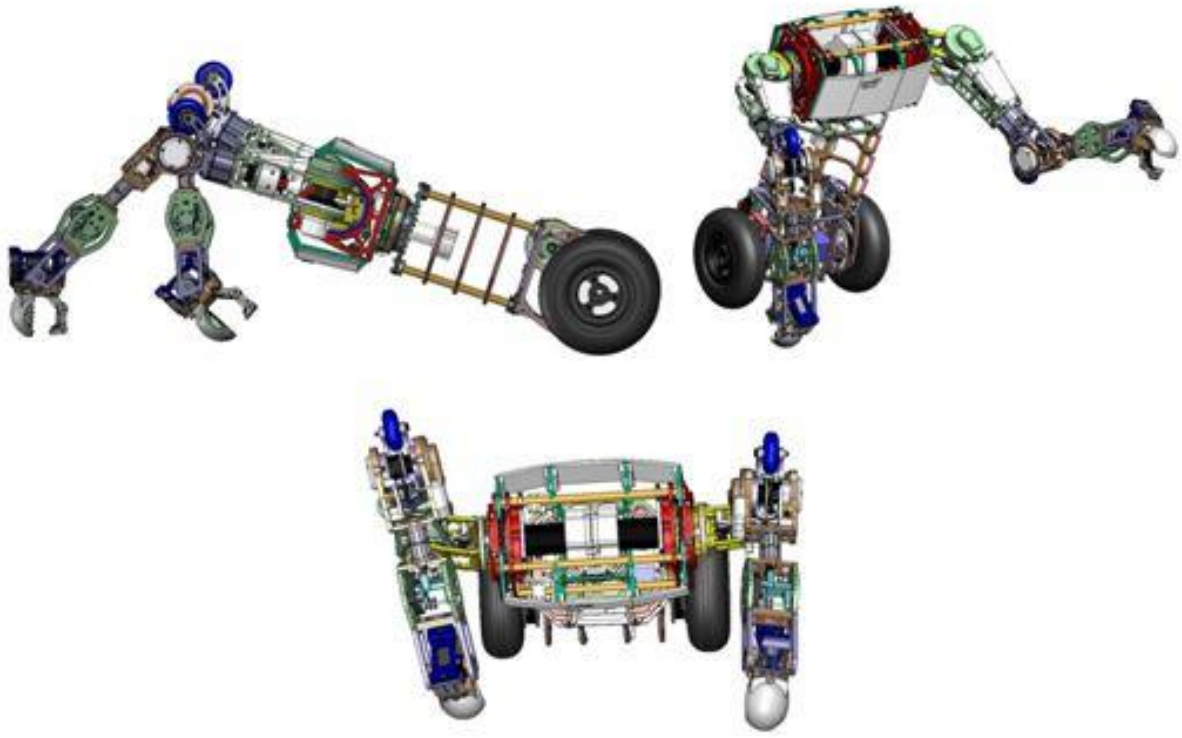

Figure 11 - Clockwise from top left: quadrupedal walking, tri-pedal stance, transition from prone to upright position

When interacting with the physical environment, the design must also have the ability to handle shock loading in the extreme case when the robot loses balance and falls on its hands. The specifics of this shock loading requirement are derived from the weight and height of the robot and are detailed in Table 1. Other requirements detail the grasping tasks that the end effector must perform in order to demonstrate its function as a manipulator. Finally, the end effector must be weight efficient for practical implementation onto the uBot-7. Note that these specifications are derived from the uBot-7 for the purpose of prototyping and validation; in the larger picture, the morphology of this end effector can be adapted to other robots with different requirements.

The objectives of this thesis are to present the framework for an initial design for a manipulator with grasping and locomotion capabilities. Without a preliminary prototype to work from, the primary requirements are focused on the physical requirements of the prototype. Secondary requirements revolve around system architecture and control scheme, which can be developed further in future work. A detailed list of the specifications is presented in the table below.

Table 1 - Specifications

	Target	Accepted
Demonstrated Grasps	Cylindrical, sphere, pinch, hook, flat	Cylindrical, sphere, pinch, hook, flat
Maximum Sustainable Impact	30 kg from 0.5 meter	30 kg from 0.25 meter
Total Weight	< 0.5 kg	< 1.0 kg
Shapes Grasped	Computer mouse, water bottle, computer mouse, tennis ball, notebook, screwdriver, etc. [16]	cup
Compliance of Finger pads under 10 N load	16mm	5 mm
Wrist flexion	45 deg	20 deg
Wrist Extension	25 deg	10 deg
Total Length (elbow to tip)	>35 cm	> 30 cm
Maximum Load	30 kg	15 kg
Series Elastic Wrist, energy absorbed	30 J	20 J
Series Elastic Wrist, detect ground contact	Yes	Yes
Rigid Finger Length	10 cm	14 cm

Following the specifications, the final design of the robotic hand with key features is displayed in Figure 12.

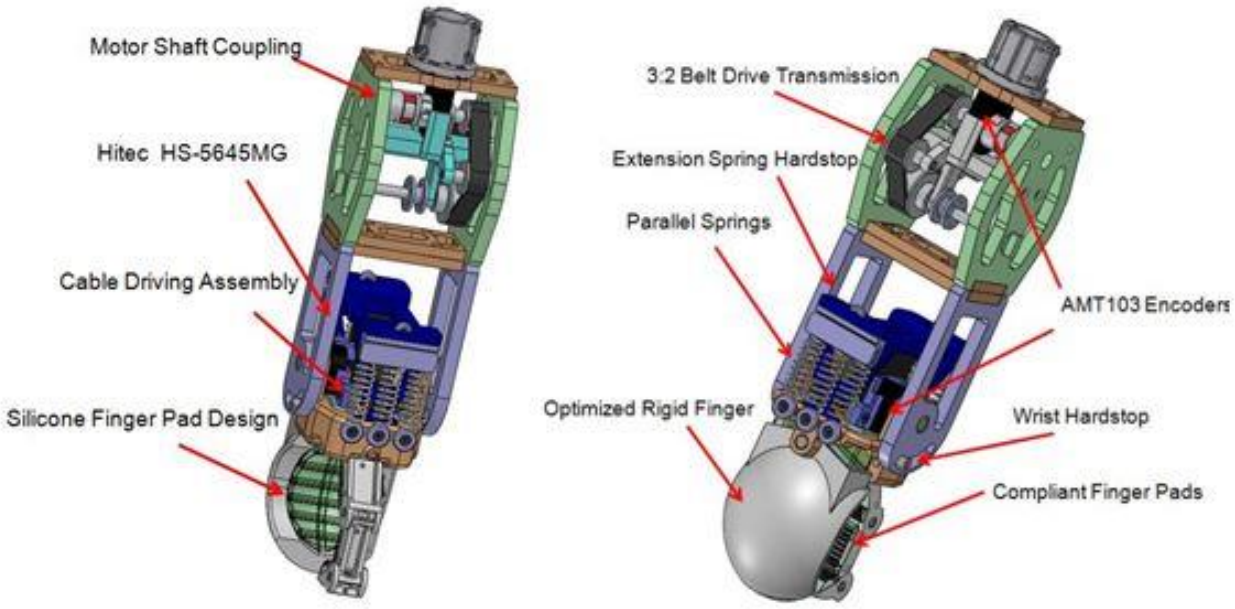

Figure 12 – Prototype key features

The design was inspired by the Model M2 hand developed at the Yale GrabLab [16]. Details of the design process of the prototype and each of its sub assemblies are discussed in the next sections.

B. Gripper Sub-Assembly

The surplus of literature available detailing the designs of various robotic hands shows the design space for these end effectors is large. Even with the specifications for this thesis, the number of possible design solutions is still large. To narrow the design space, the majority of robotic hand morphology is categorized into anthropomorphic hands and non anthropomorphic hands. Generally the anthropomorphic morphology is selected because the ultimate goal of most robotic hands is to achieve the same level of dexterity and capabilities as the human hand. However, this approach can be dangerous because the design complexity exponentially increases as a robotic hand attempts to achieve the same capabilities as the human hand. The weight

restriction for this design makes complex designs undesirable. As a result, the best design to meet these requirements is driven by efficiency, where any increase in complexity must yield a greater increase in functionality. This design concept is adapted from Ciocarlie's organization of robotic hand design through the comparison of the capability of certain hands to their complexity. Efficient designs are determined by the slope of the curve, where high efficiency correlates with a high slope. This concept is illustrated in Figure 13 below.

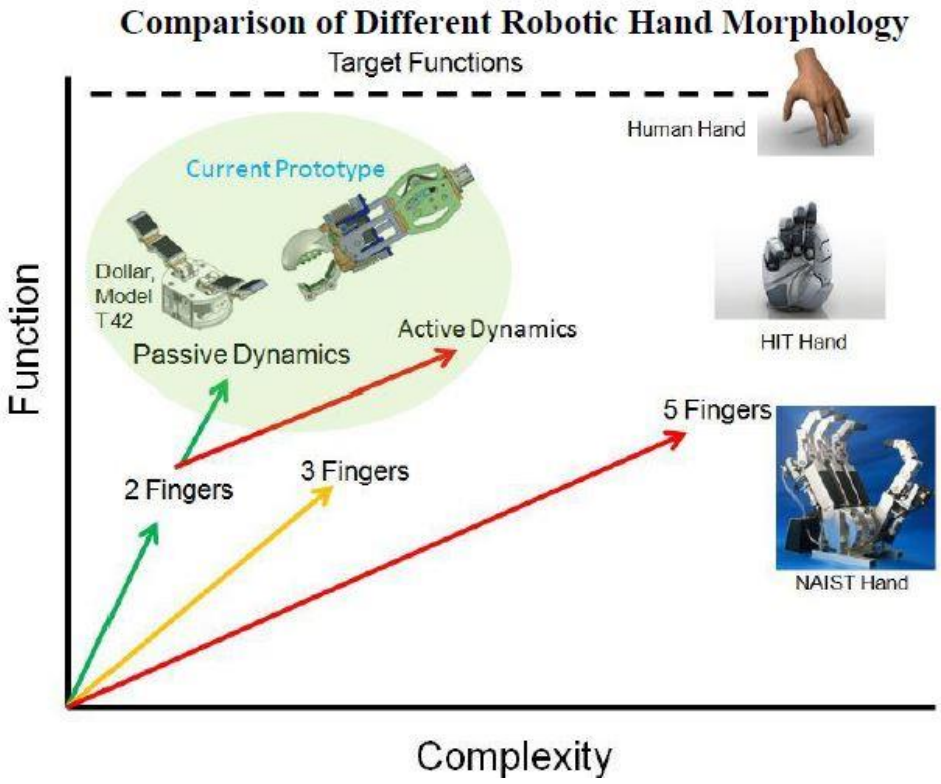

Figure 13 - Comparison of different hand morphology

At the basic level, a two finger gripper is a simple design that is versatile in its ability to grasp objects. The introduction of passive mechanics increases the two finger gripper's grasp space without a significant increase in complexity. The primary methods of passive mechanics used in this prototype are underactuation and compliant finger pads. An underactuated mechanism allows the finger with multiple degrees of freedom to be driven by a lower number of

actuators. Where direct actuation of each degree of freedom would require complex planning and additional sensing to achieve a stable grasp, underactuation can reduce planning complexity through passively conforming to the shape of an object. The compliant finger pads increase the subspace of arbitrary shapes that the manipulator can grasp by adding additional compliance to the fingers.

With an underactuated two finger gripper design selected for the final design, the next step is to adapt the morphology for locomotion. The adapted design is inspired by the M2 Dollar hand, which is a two finger gripper with an active finger coupled and a rigid finger for gripping. The active finger provides the gripping force meanwhile the rigid finger provides a surface for contact. From this type of morphology, the rigid finger shape can be altered to sustain the required external loads. A spherical design was determined to be the ideal shape for the rigid finger. The advantage of sphere morphology is its continuous curvature, which provides consistent contact characteristics with the ground regardless of the position of the finger in space. The consistent contact characteristics help to linearize the dynamics of the system which simplifies the design of a controller for the system. Any discontinuity along the surface of the rigid finger changes the behavior of the system, requiring an adaptive controller or a multiple state controller. Figure 14 below illustrates the difference between the discontinuous surface and smooth surface.

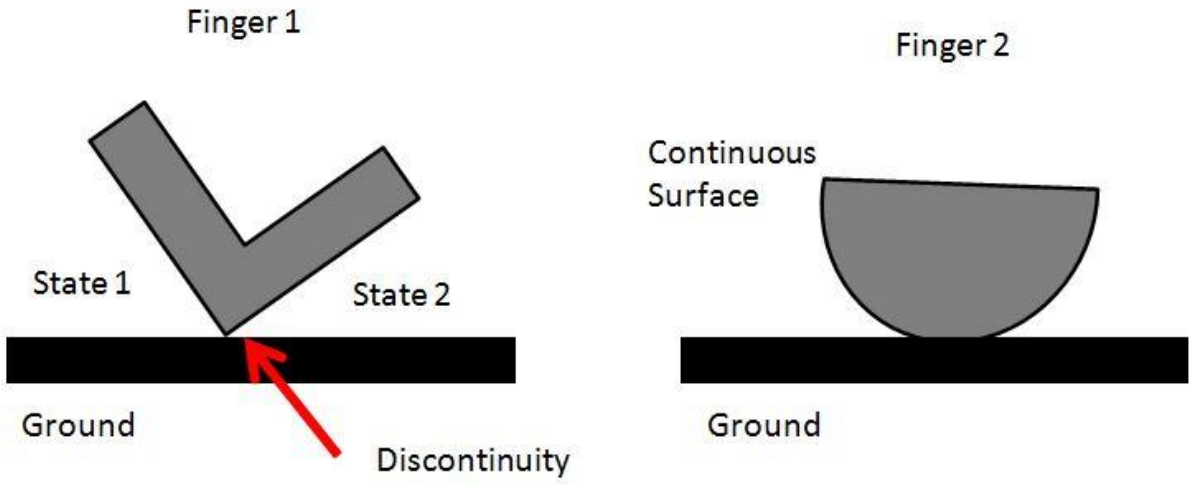

Figure 14 - Illustration of different finger contacts with the ground

The rigid finger is designed to sustain dynamic loads for quadrupedal motion. The most extreme loading condition that the uBot-7 may experience is an impact load from losing balance. Using finite element analysis, the rigid finger is optimized to sustain an impact from a 30 kg mass (the weight of the uBot-7) dropped from a 1 meter height (approximate height of the uBot-7). This loading scenario is an overestimate because the center of mass for the uBot-7 is located below its head and the trajectory of the uBot-7's fall does not follow the path of a vertical drop but more of a circular motion about a center of rotation. However, finite element analysis for dynamic loads can be inaccurate and 3D printed materials often have weaker material properties than their non-3D printed counterparts. The marginally accepted impact condition was determined by estimating the impact energy when the robot tips over while its arms are 90 degrees from its body, shown in Figure 15.

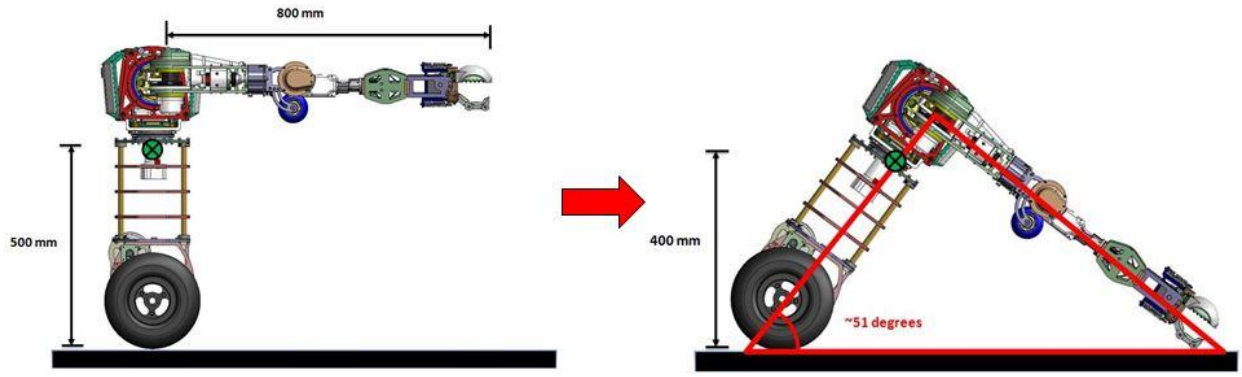

Figure 15 - uBot-7 falling with arms at 90 degrees

C. Design Optimization – Rigid Finger

Two optimization features in ANSYS were implemented for designing the rigid finger. The first optimization feature was a response surface approach. For this approach, critical parameters are selected for optimization along with a specified range of values for those parameters determined by geometric constraints. After determining the objectives for optimization, which were weight and factor of safety for this design, a design of experiments given those parameter value ranges was set up and a response curve was calculated to fit the design points produced from the design of experiments. The local minimum on the response curve represents the optimal parameters that minimize the weight of the finger while satisfying the safety factor requirement. This local minimum is found using nonlinear programming by quadratic Lagrangian (NLPQL), a gradient based search algorithm that is ideal for single objective optimization problems with multiple constraints. This method is limited by the accuracy of the response curve and the number of different starting points that are used for the NLPQL. Using this method for optimizing a dynamic analysis of the rigid finger proved unreliable because the program was unable to accurately fit a response curve to the design points. The accuracy of the curve is displayed below in Figure 16.

Table of Schematic D3: Response Surface

	A	B	C
1		P9 - Solid Mass	P14 - Safety Factor Minimum Minimum Value Over Time
2	Coefficient of Determination (Best Value = 1)		
3	Learning Points	0.99525	0.77611
4	Root Mean Square Error (Best Value = 0)		
5	Learning Points	0.0011404	0.00076234
6	Relative Maximum Absolute Error (Best Value = 0%)		
7	Learning Points	10.891	75.28
8	Relative Average Absolute Error (Best Value = 0%)		
9	Learning Points	5.498	39.776

Figure 16 - Accuracy of the response curve to the design of experiment points

Note the large estimation errors for the safety factor of the design. As a result, the direct optimization feature in ANSYS using an adaptive single-objective method was implemented instead, which is a relatively brute force method of optimization. Given the parameter range, the direct optimization calculates a number of initial guess points and then changes each parameter incrementally to determine the change in mass of the finger. Similar to NLPQL, the adaptive single-objective method uses a gradient based algorithm for searching the design space. However unlike the NLPQL, this method attempts to find a global optimum. This optimization feature is time intensive compared to the response surface, but the results are more reliable because the outputs are calculated directly from the model setup. The output of the direct optimization is displayed below in Figure 17. The details of the optimization process can be found in Appendix A.

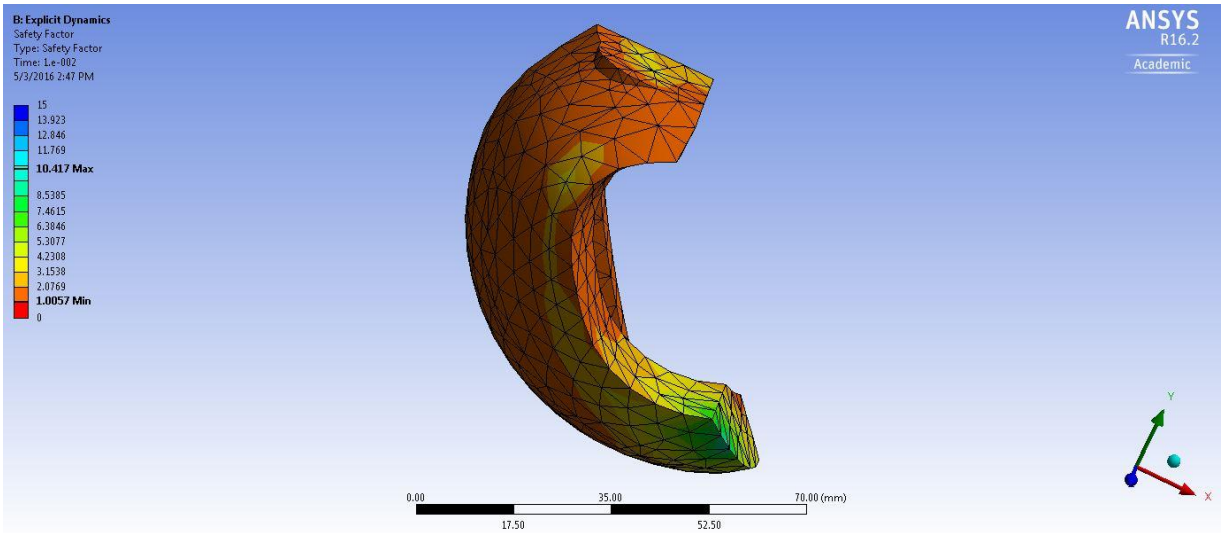

Figure 17 - Validation of optimization results

The supporting plates that make up the forearm and wrist section of the prototype were also analyzed in ANSYS for structural safety under impact loads. The plates were simulated under a static load with a target safety factor of 3 to compensate for dynamic loads. The parts were analyzed in this manner because the distribution of energy throughout the system during impact loads was unclear. The analysis of those structures is displayed in Appendix B.

D. Compliant Finger Pad Design

The c-shape design of the rigid finger gives space to insert compliant finger pad material. For a stable grasp, compliance is necessary for two reasons. The first is that the increase in surface area improves the stability of the object by introducing opposing moments against any rotation. This concept is illustrated in Figure 18.

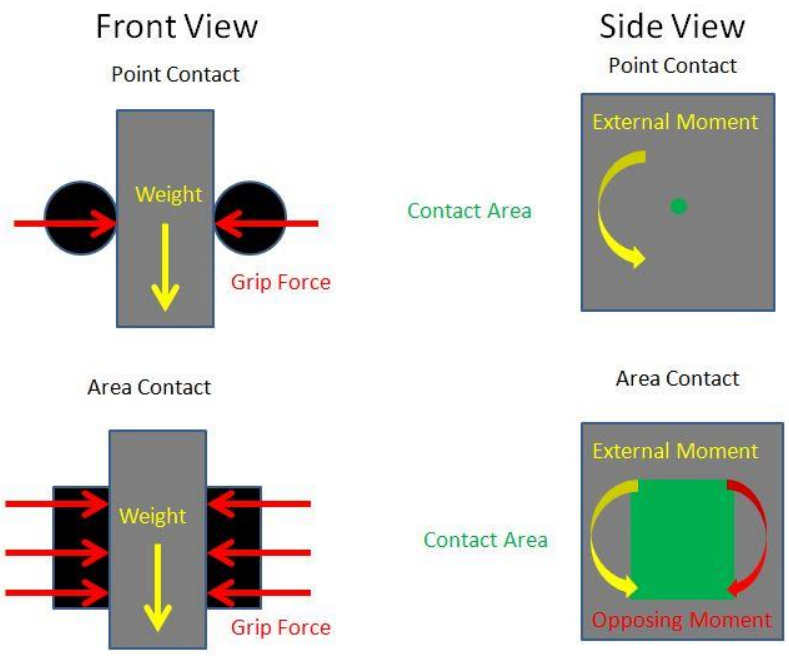

Figure 18 - Illustration of point contact grip versus area contact grip

The second advantage of compliance is that it improves the ability of the hand to grasp objects of arbitrary shapes without the need for complex planning algorithms. The compliant material selected is Dragonskin FX-Pro, a silicone rubber that is fabricated through molds. Dragonskin FX-Pro was selected because of its extremely low durometer rating of 2A, which is ideal for a high level of compliance. This level of compliance is necessary for this design because the active finger exerts a low grip force on the grasped object. Material data for the Dragonskin FX-Pro silicone rubber is displayed in Figure 19 below.

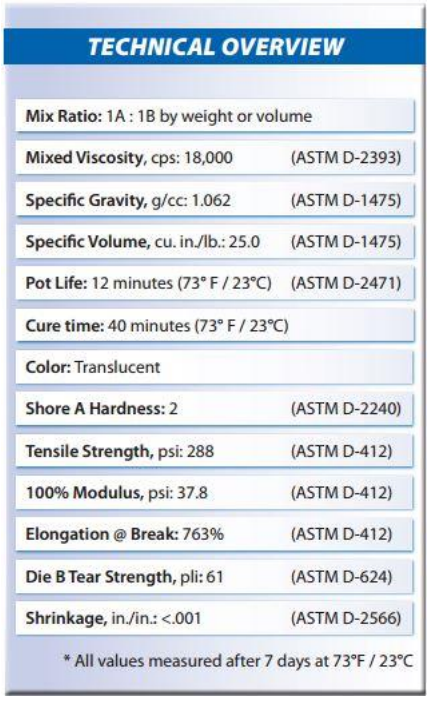

TECHNICAL OVERVIEW

Mix Ratio: 1A : 1B by weight or volume	
Mixed Viscosity, cps: 18,000	(ASTM D-2393)
Specific Gravity, g/cc: 1.062	(ASTM D-1475)
Specific Volume, cu. in./lb.: 25.0	(ASTM D-1475)
Pot Life: 12 minutes (73° F / 23°C)	(ASTM D-2471)
Cure time: 40 minutes (73° F / 23°C)	
Color: Translucent	
Shore A Hardness: 2	(ASTM D-2240)
Tensile Strength, psi: 288	(ASTM D-412)
100% Modulus, psi: 37.8	(ASTM D-412)
Elongation @ Break: 763%	(ASTM D-412)
Die B Tear Strength, pli: 61	(ASTM D-624)
Shrinkage, in./in.: <.001	(ASTM D-2566)

* All values measured after 7 days at 73°F / 23°C

Figure 19 - Material properties of Dragonskin FX-Pro

Compliance of the finger pad is typically determined by the properties of the material used. However, with the same material, additional compliance can be achieved by altering the geometry of the finger pad. This additional degree of freedom is suitable for the rigid finger for this prototype, which has the space in the hollow center of the c shape for removing material for different designs. As a proof of concept for the potential for this type of finger pad, simple circular cuts were spaced evenly throughout the finger pad. Simulations of the material behavior were conducted in ANSYS using imported material properties from a uniaxial test of the silicon. The mechanical behavior of the silicon was approximated using the Arruda-Boyce model. This approximation is the most accurate for predicting the material properties of hyperelastic material using minimal experimental data. A comparison of the curve fit to experimental data is given in Figure 20 below.

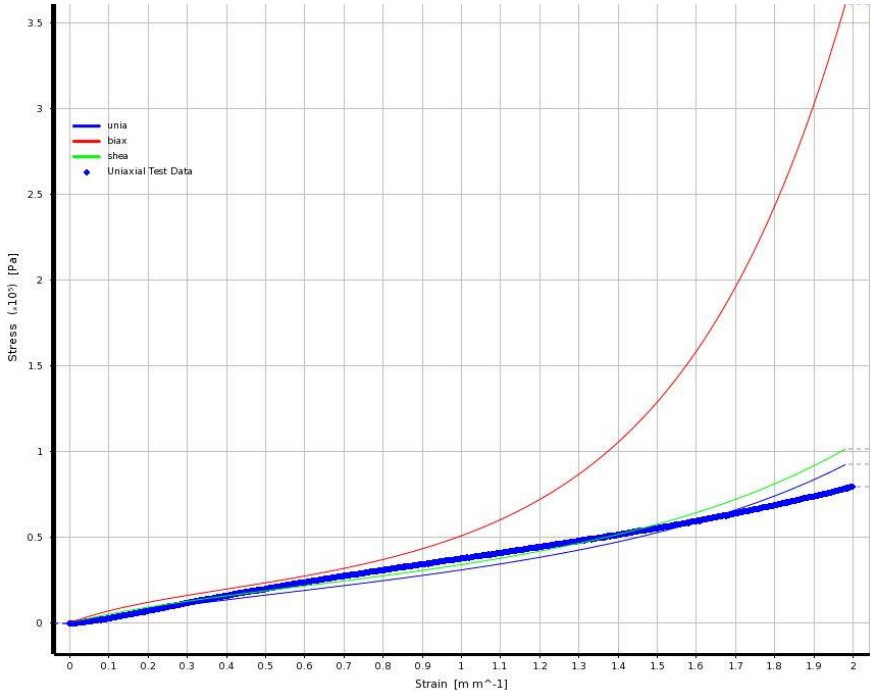

Figure 20 - Arruda-Boyce approximation of uniaxial test data for Dragonskin FX-Pro

Simulations of the silicon with complex geometries were unable to converge to a solution 9 seconds into the analysis. Around 8 seconds the total strain in the material was around 0.7, which was within the linear region of the material. To circumvent the convergence problem, the hyperelastic material data was linearized because the material was not experiencing strains outside of the linear region. The geometry was also broken down into a single unit cell with a hole in the middle.

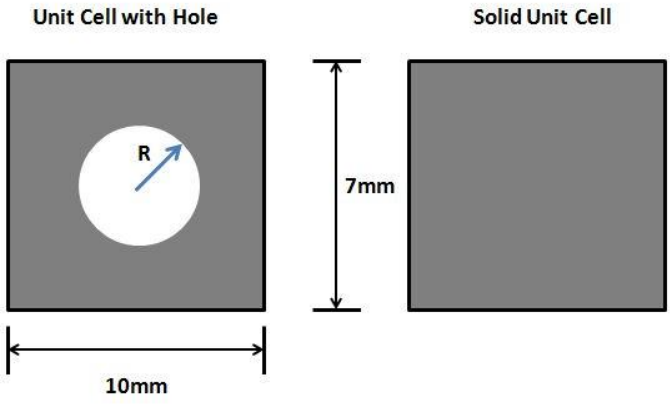

Figure 21 - Unit cell with hole and solid unit cell

Due to the volume constraints placed on the finger pad by the optimized rigid finger, the dimensions for the unit cell were set to 7 mm x 10 mm x 10 mm for the best distribution of the holes throughout the finger pad. A 1.0 N load was applied to the unit cell with frictionless supports added to the adjacent faces to the hole to approximate the relationship of the unit cells stacked side by side.

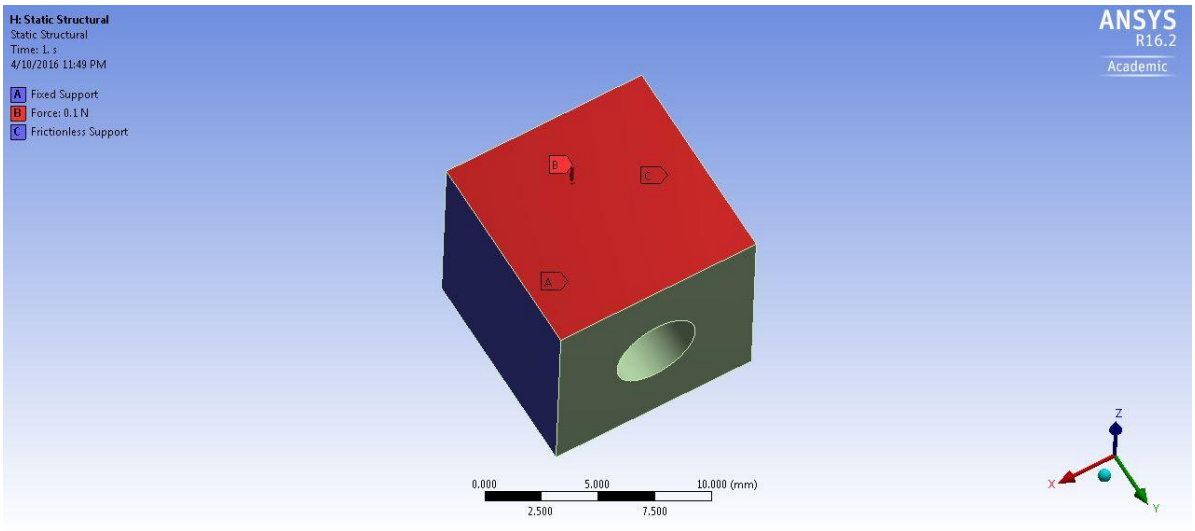

Figure 22 - FEA setup for unit analysis

By simulating the behavior of the unit cell, an equivalent elastic modulus for a solid unit cell could be predicted as a function of the hole radius. This calculation was derived by comparing the stiffness behavior of the two unit cells and approximating the effective elastic modulus so that the stiffness is equivalent. The effective elastic modulus of the solid unit cell had a stiffness value with 1% of the stiffness of the unit cell with the hole at the center. A plot showing the effective elastic modulus of the solid unit cell as a function of hole radius is shown in Figure 23 below. Appendix C displays the tabulated data used to determine the plot in addition to the estimation errors.

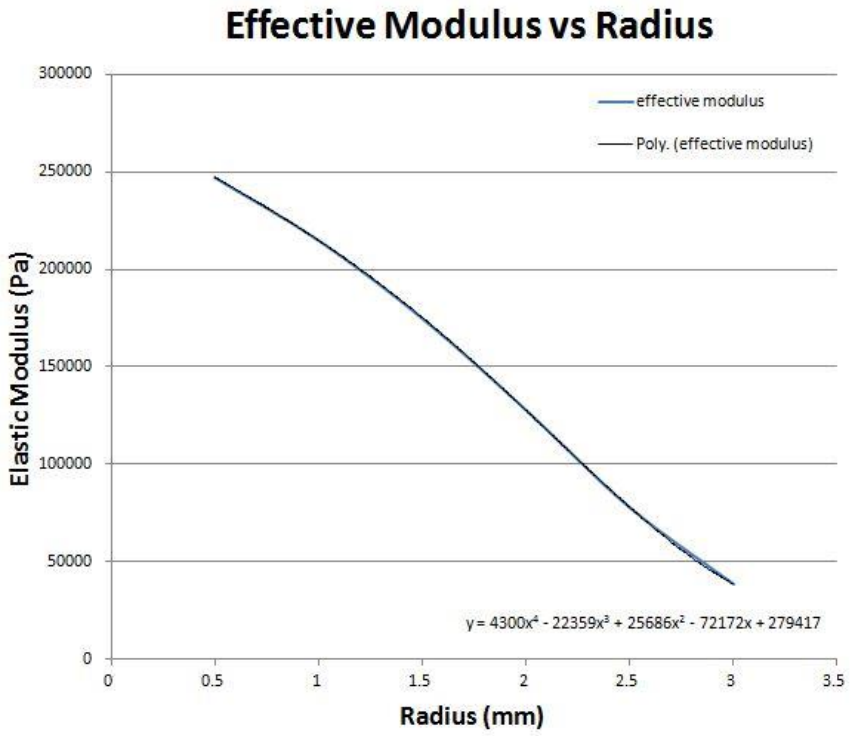

Figure 23 - Effective modulus (Pa) as a function of hole radius (mm)

A fourth order polynomial function was selected to curve fit the data. This was the lowest order function that produced an average error of less than 1% with respect to the unit analysis data. The results of this curve fit produced a function given below,

$$E(r) = 4300r^4 - 22359r^3 + 25686r^2 - 72172r + 279417 \quad (1)$$

where E is the effective elastic modulus in Pascals and r is the radius of the hole in millimeters. Using this derived function, the geometry for the finger pad was simplified to a solid material with an elastic modulus determined from the function. The effective elastic modulus was determined based on the desired compliance of the finger pad. This diameter of the holes could then be calculated using Equation 1. The finger pad and rigid finger assembly was fabricated using the hybrid deposition manufacturing. The rigid finger was 3D printed using ABS and the

silicon finger pad was molded directly onto the rigid finger. The unique aspect of this design is the use of a dissolvable mold in order to achieve the complex geometry of the finger pad. The dissolvable mold was 3D printed using HIPS plastic. 3D printing the mold increased the design freedom for the finger pad material and allowed for certain shapes that were unattainable through conventional molding techniques. Figures for this process are displayed below in Figure 24.

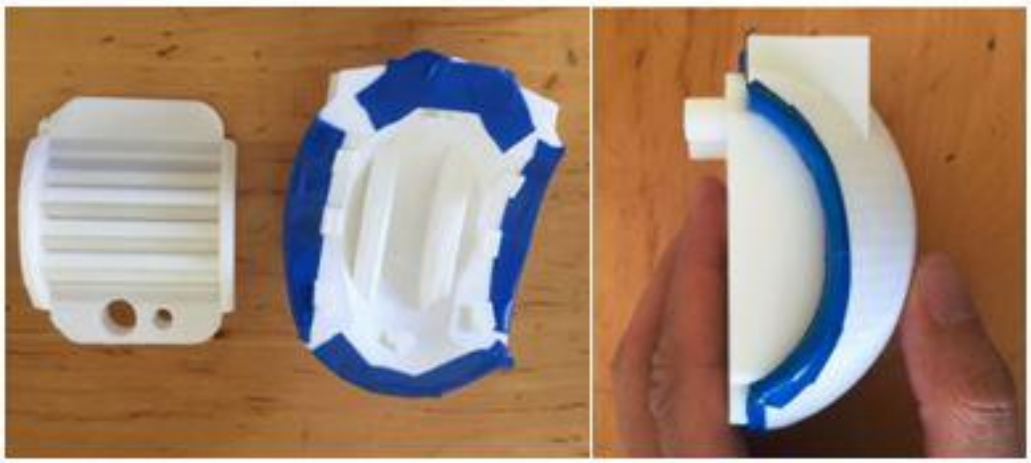

Figure 24 - Dissolvable mold and rigid finger assembly

E. Active Finger Design

For the active finger, the design choice is limited to either a two linkage assembly or a three linkage assembly. Any additional link increases the complexity of the design without adding any tangible benefit other than increasing the area of contact. Comparing the capability to complexity ratio for the two assemblies, the two linkage design maximizes efficient because it provides the bare minimum of two points of contact for a grasp and a third point of contact to fix the object from translational motion in a 2D plane. A three link systems adds an additional point of contact which is not required for fixing translational motion. However, it is difficult for a two link system to pick up thin flat objects without increasing the dimensions of each link so that the

effective length of the active finger significantly exceeds the length of the rigid finger. As a result, the three link finger is selected over a two link finger, where the trade off to design efficiency is an increase in capability.

A kinematic analysis of the three link active finger and flat surface rigid finger is performed to determine ability of the end effector to perform the target grasps. The Kutzbach Criterion is used to determine the mobility of the gripper system to determine if the specified grips are achievable with a single actuator. The mobility formula in 2D space used to determine if the Kutzbach Criterion is satisfied is given below,

$$M = 3(N - 1) - 2f_1 - f_2 \quad (2)$$

where M is mobility, N is the number of links in the system, f_1 is the number of joints with 1 degree of freedom, and f_2 is the number of joints with 2 degrees of freedom. Proof that the different grasps can be achieved for a 3 link system with 1 actuator is displayed in Appendix D.

Dimensions of the active finger were determined according to the maximum allowable size for the rigid finger. For grasping conventional objects with significant dimensions along the three principal axes, the total length of the active finger can be as long as the rigid finger to achieve a stable grasp. However, grasping thin, flat objects that only possess significant dimensions along two principal axes requires the active finger to be longer than the rigid finger. This requirement introduces a design tradeoff between the prototype's manipulation ability verses its locomotion ability. Extending the length of the active finger increases the prototype's ability to grasp objects at the cost of reducing its ability to survive loading under locomotion conditions because the active finger can not be completely protected by the rigid finger. For this

prototype, the dimensions of the active finger were selected so that the length of the distal phalange was minimized while the proximal and middle phalange were maximized, all while minimizing the total length of the finger. The distal phalange was minimized because its purpose was only to grasp flat objects and provided little support for the remaining target grasps.

F. Cable Driver Sub-Assembly

An effective gripper must be able to hold objects for an extended period of time without causing damage to the actuators. If the actuator is connected directly to the cable driving the finger, the gripper must hold a grasp by stalling the actuator. For a short duration pick and place motion, this type of direct actuation is allowable because the actuator will not overheat to catastrophic temperatures when stalled for a short duration. However, for a service robot that may be required to hold an object for minutes or even hours, stalling to maintain a stable grasp can overheat the motor and cause permanent damage. A solution to this problem is to utilize the passive dynamics of the actuator. Actuators have a certain hold force due to a combination of static friction and gear reduction. Even when the actuator is powered off, this hold force is still present and can be amplified to maintain tension in the cable for a stable grasp. Amplifying the hold force can also be achieved passively using the Etylewein Formula, which states that,

$$\frac{T_1}{T_2} = e^{\mu\varphi} \tag{3}$$

where μ is the friction coefficient, Φ is the angle of wrap in radians, and T_1 and T_2 represent the output and input force respectively. This equation is also known as the belt friction equation used to determine the brake force in band brakes. By introducing a capstan into the cable driving

system and wrapping the cable around the capstan before attaching it to the pulley, the hold force of the motor can be exponentially increased without the addition of any active components or increase in the power of the actuator. To prevent the capstan from impeding the actuator's ability to flex the cable, a one way clutch is introduced to allow the capstan to rotate freely in the direction of tensioning the cable but not in the direction of release. To release the cable for extension of the finger, the actuator will rotate in the opposite direction to put the cable in slack, which will allow the extension springs in the finger to release the grasp. This mechanism was designed by Kang, In, Cho and adapted for this prototype [17]. Figure 25 illustrates the concept behind this mechanism.

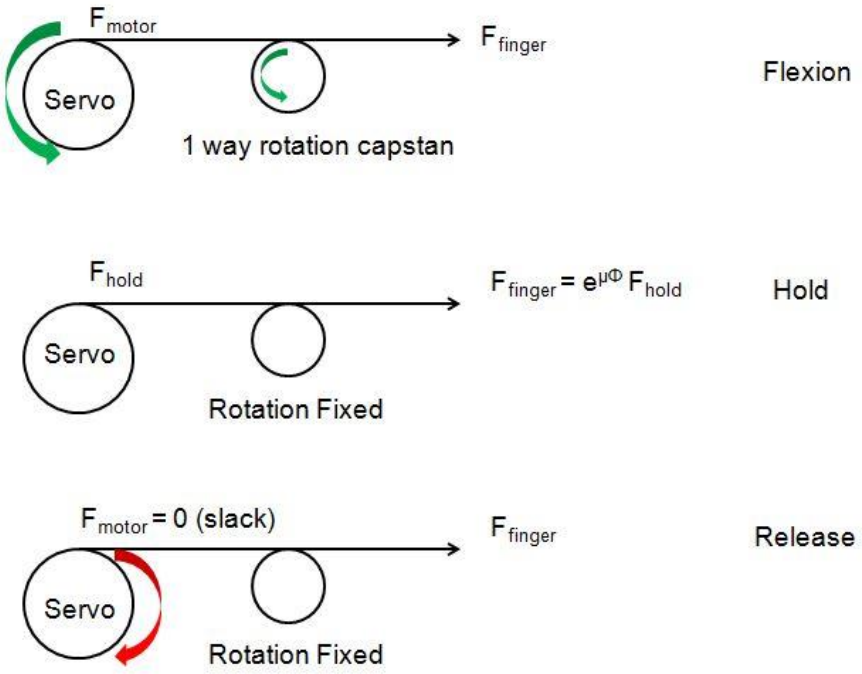

Figure 25 - Schematic of cable driver mechanism operation

The advantage of this cable drive system is that it is an energy efficient method for holding a stable grasp because it eliminates the need for the actuator to be powered for the entire duration of the grasp. This also effectively protects the actuator from overheating from stalling for an extended period of time. The disadvantage of this system is that it introduces more friction

in the flexion and extension motion of the finger. The spring constant for the extension spring must increase to compensate for the amplifying effect of the capstan even when the other end is in slack. The torque requirements for the actuator must subsequently increase to overcome the higher spring constant for the extension springs. The tradeoffs for this mechanism are qualitatively determined to be small compared its benefits. The prototype for this drive mechanism is displayed below in Figure 26.

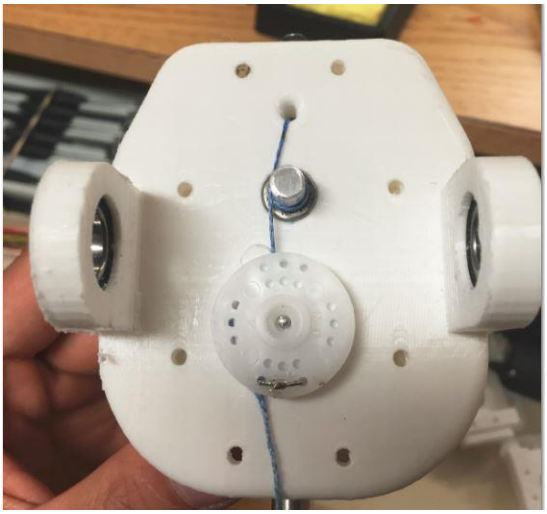

Figure 26 - Prototype of the cable driver mechanism

An experiment was designed in order to validate this cable driving mechanism and to empirically determine the number of wraps that would be required. Theoretical calculations were determined to be impractical because there was not a reliable method for determining the friction coefficient between the aluminum and cable. Instead, the hold force was estimated empirically. The results of the experiment are presented in Table 2.

Table 2 – Hold force related to the number of wraps. A 711 g weight was attached to the finger

Number of Wraps	Hold Force, N (lbf)
0	28 (6.4)
1	18 (4.0)
2	5.3 (1.2)
3	0.93 (0.21)

The object in the figure was a known mass that was placed at the same location of the finger for every wrap. The results of the experiment show that three wraps around the capstan will amplify the hold force enough to grasp the target objects.

Note that Figure 26 displays a specific cable routing design, which was introduced due to the limitations of the actuator for the active finger. The selected actuator for this prototype was a Hitec HS-5645MG servomotor because it satisfied the torque and power requirements for the different target grasps in a compact form factor and economic price. The specific servomotor was limited to 120 degrees of motion, which was below the angular distance necessary to fully flex the finger with the given pulley diameter. To increase the distance, the cable was routed to wrap around a second capstan positioned under the pulley. Figure 27 illustrates this routing method.

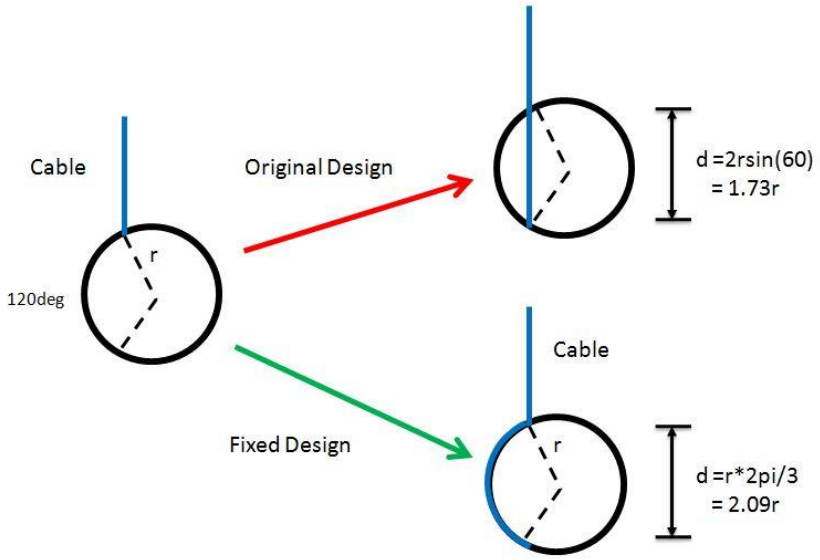

Figure 27 - Illustration of the cable routing

The current method for cable routing is not a long term solution because the friction between the cable and the plastic decreases the efficiency of actuator and increases the wear rate of the part and the cable.

G. Series Elastic Wrist Sub-Assembly

Series elastic actuators have two advantages over springless actuated systems. The first advantage of the series elastic actuator is protection against shock loading. Shock loading represents the worst case scenario in applications for locomotion, where gear transmissions are typically at the highest risk for failure. The spring component of a series elastic actuator can absorb a proportion of the energy from shock loads, thereby protecting the gear transmission from failure. The second advantage of series elastic actuators is the system's potential for sensing. By adding sensors to measure the deflection in the spring, a series elastic actuator can be used to determine contact with the environment. For this prototype, the series elastic actuator allows the hand to detect when it makes contact with the ground.

Design of a series elastic actuator is typically an optimization problem, where the motor and spring must be selected to meet size constraints while achieving the desired shock protection and speed. Springs with high stiffness increase the bandwidth of the series elastic actuator at the cost of decreasing its potential for shock protection. For this prototype, size constraints determined the selection of the individual components. The motor selected is a Maxon EC 32 flat 6W motor with a Maxon GP 22 planetary gearhead. Detailed calculations verifying the selection of the wrist motor and servomotor are shown in Appendix E. The motor was selected for its small form factor while achieving the necessary power requirements for the wrist. The gears are made of steel which has a fracture toughness in regards to impact of approximately 30 J. Selection of the spring is detailed in Appendix F. The spring was selected according to the required shock absorbance and extended length constraints of the design.

H. Design for Additive Manufacturing

The majority of the prototype was designed to be fabricated using the EOS Formiga P110 selective laser sintering machine with P2200 Performance 1.0 nylon power. Details of the material property of the nylon power are displayed in Figure 28 below.

PA 2200 Performance 1.0 | PA12			
Mechanical properties	**Value**	**Unit**	**Test Standard**
Tensile Modulus	1700	MPa	ISO 527-1/-2
Tensile Strength	50	MPa	ISO 527-1/-2
Strain at break	20	%	ISO 527-1/-2
Charpy impact strength	53	kJ/m²	ISO 179/1eU
Charpy notched impact strength (+23°C)	4.8	kJ/m²	ISO 179/1eA
Flexural Modulus (23°C)	1500	MPa	ISO 178
Izod Impact notched (23°C)	4.4	kJ/m²	ISO 180/1A
Shore D hardness (15s)	75	-	ISO 868

Figure 28 - Material properties of PA200 Performance 1.0

The nylon power possesses the desired strength to weight ratio that allows the prototype to reach the weight specification while supporting the uBot-7. The laser sintering method allows complex geometries with overhangs to be printed without additional support material that must be broken off. Without extra supports, the finish of the printed piece is finer than conventional printers. Due to the cost of the nylon material and the printer, the actual prototype was manufactured using Makerbot Replicator series printers. The Replicator series is a low cost but also low resolution alternative to the Formiga, which made the Replicator printers better suited for initial prototypes.

Additional design considerations had to be taken into account to compensate for the low resolution of the Replicator printer and the support material that would be printed for overhangs. Due to the material properties of the PLA and ABS material typically used by the printers, the plastic will typically expand a little after it is printed. For parts that require specific dimensions in order to fit together, the dimensions specified in the CAD model must be offset by 0.2 mm to

0.4 mm to account for the expansion of the plastic after it is printed. Additionally, the relatively open print environments of the Replicator printers put printed parts at risk of warping. Closed print beds such as the Replicator 2x or the Replicator z18 mitigate warping to negligible levels. Printing the dissolvable molds required the Replicator printers with heated print beds and closed environments because HIPS plastic warps easily compared to PLA or ABS. For speed and cost, all parts were printed at densities ranging from 10% to 20%. While the final prototype was intended to be printed with the Formiga, unforeseen circumstances made the Formiga unavailable for use prior to the completion of this thesis. When the Formiga printer becomes available, the CAD models for the prototype parts must be adjusted to account for the higher resolution of the Formiga compared to the Makerbot.

IV. Evaluation

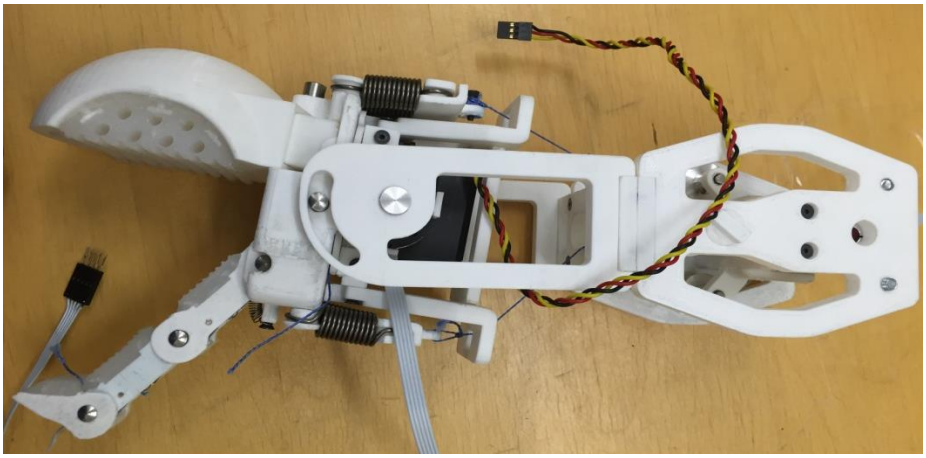

Figure 29 - Physical Prototype

The total weight of the prototype was estimated to be about 0.61 kg. Calculations for the weight are shows in Appendix G. The length of the final prototype was around 31 cm, which was shorter than the target length. The small size is not an issue however because the arm length can be easily extended by adding a shaft between the connections at the elbow joint.

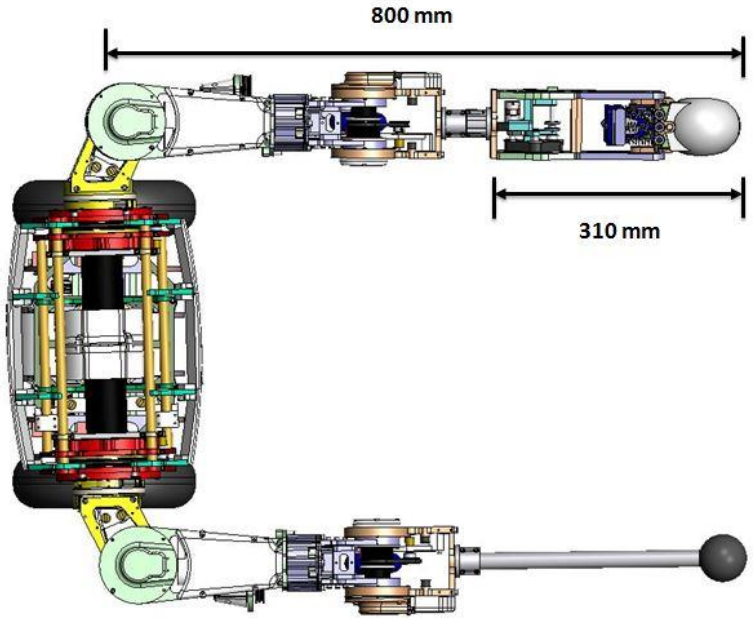

Figure 30 - Dimensional comparison between prototype and original end effector

A. Grasping Performance

Grasping performance was determined empirically. The target objects listed in the specifications were each laid on a table and the prototype was manually positioned to grasp the object. A grasp was determined to be stable if the object did not slip as the hand translated or rotated in 3D space. Some images demonstrating the target grasps are displayed below in Figure 31.

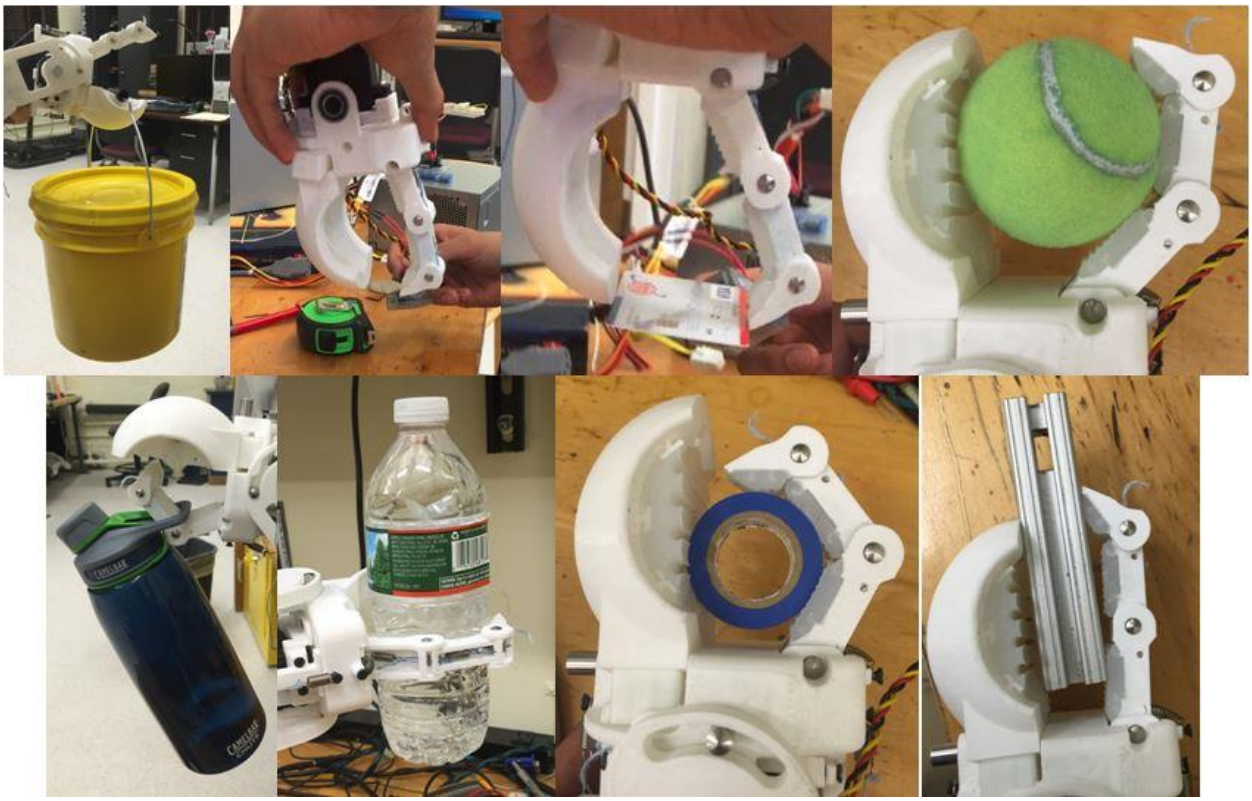

Figure 31 - Grasps from top left: nonprehensile, pinch (quarter), pinch (card), sphere, hook, cylindrical, underactuated, pinch (long object)

As predicted, the addition of the third link in the finger allowed the prototype to pick up thin, flat objects from a surface. Underactuation of the finger is also demonstrated with smaller objects that allow the finger to conform to the shape. The underactuated grasp is demonstrated in the grasp of the blue electrical tape. The prototype was also able to perform a stable grasp of a 16 fluid ounce water bottle, which was the benchmark target weight for the prototype.

The cable driving mechanism was tested by cutting the power to the motor while the prototype was holding an object. It was found that the finger would slip whenever the power was turned off, which caused the prototype to lose its grasp of the object. One explanation for this behavior is that the force opposing the finger from the grasp is high enough to cause the cable to slip around the capstan and backdrive the motor. This can easily be fixed by adding an additional wrap around the capstan. Another possible explanation is that at the instant when the power is cut off, the servomotor reads a PWM signal that causes it to rotate to a different position. For testing, the servomotor is driven by a HPP21+ Digital Servo Programmer, which is a separate device that allows the user to manually control the duty cycle of the PWM by turning a potentiometer. It is possible that the programmer can alter the duty cycle when power is cut from it. To circumvent this problem, the servomotor will be controlled by the dsPIC33 instead.

B. Compliant Behavior of Finger Pad

To validate the results of FEA on the silicone rubber, a compression test was performed using an Instron Universal Testing machine. The fabricated finger pad was fixed parallel to the ground and was loaded to 10 N in compressions with a specimen of a known surface area. The setup for this experiment is displayed below in Figure 32.

Figure 32 - Experimental setup for silicone finger pad test

The results of the experiment were compared to the deflection behavior predicted in the finite element model. For a 1.0 N load, the predicted directional deformation had a 5.7% error compared to the experimental value. For a 10 N load the predicted directional deformation had a 40% error.

C. Series Elastic Wrist Performance

The evaluation metrics for the series elastic actuator were based on its usability for the uBot-7. One of the functions that the wrist had to achieve was ground contact sensing. To demonstrate this ability, a basic circuit was setup using a dsPIC33FJ64MC202 microcontroller. The two AMT103 encoders and two LEDs were connected to the PIC, where the LEDs were programmed to light up when the hand made contact with the ground.

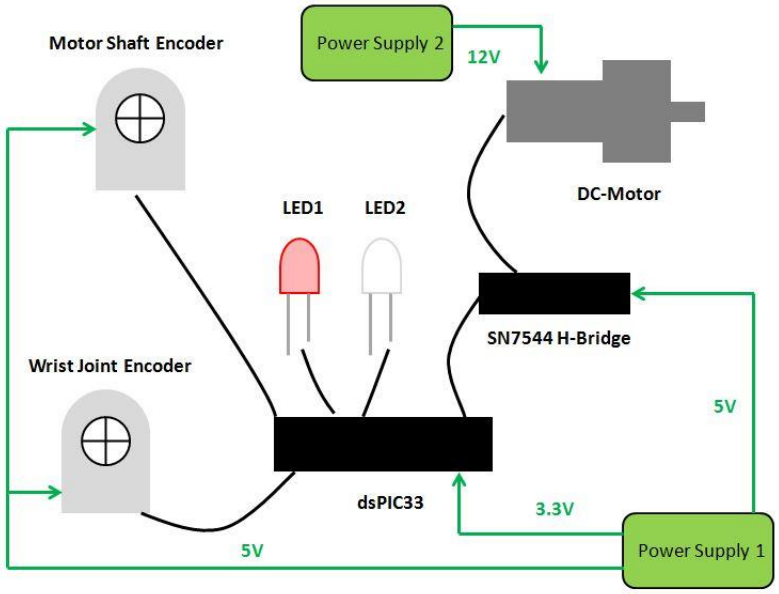

Figure 33 - Schematic of circuit for drive and control of the prototype

The quadrature encoders were set to the maximum resolution of 2048 to measure small deflections in the series springs. Detailed calculations shown in Appendix F indicate that the minimum deflection in the spring is approximately 12 mm which corresponds to approximately 10 degrees of rotation about the wrist. This angle is well within the range for the encoder to measure position accurately.

Designing a proper controller for the series elastic wrist requires proper system identification of the prototype. This work is currently outside of the scope of this thesis, however it is important to demonstrate possibility of implementing closed loop control onto the device. The LED lights were used to ensure that both encoders were measuring position and velocity. For a proof of concept, the code for a full state feedback position controller is programmed into the dsPIC33 with the parameters arbitrarily defined. A calibration function was also included in order to zero the position of the wrist joint. For future work, the parameters will have to be tuned based on the results of system identification and the desired bandwidth of the system.

V. Discussion

A. Grasping

Overall, the prototype was able to meet the specifications for grasping the target objects. However, the current design introduces a significant amount of friction around the joints of the finger and servomotor that is driving the cable. As a result, the prototype produces a grip strength that is smaller than the capabilities of the servomotor. Currently the joints for the finger are made of press fit dowel pins that keep the links connected and in position. The proximal phalange and the distal phalange pin holes are designed so that the dowel pin is fixed, while the middle phalange has pin holes that are slightly larger to enable rotation. Due to the low resolution of the Makerbot and the supports that were printed during fabrication of the finger parts, there is still significant friction between the dowel pin and the middle phalange hole despite the tolerances factored into the design. Fabricating the finger links using a higher resolution printer that does not print supports can reduce friction at the joints, but a better solution may be to introduce bearings at the joints. As the cable moves up the finger from the proximal phalange to the distal phalange, the effects of friction is compounded. Due to the compounding effect, the finger is unable to bend unless an object is introduced to force the finger to bend to conform to the shape. While this aspect of the finger does not affect the grasping performance of the prototype, it may penalize the prototype's locomotion potential. The inactive state of the finger is at an open grip due to the extension springs that are required to passively release the grip. At its open position, the finger is at risk for damage during locomotion unless it can retract closer to the rigid finger. Originally, the prototype was designed so that during locomotion the finger would close and the motor would turn off so that the active finger would be protected from the external environment by the rigid finger. However, the active finger was designed to be slightly longer than the rigid

finger in order to grasp flat objects; without the ability to actively bend, the active finger loses protection from the rigid finger in the closed position. The solution to this problem is to either reduce the friction at the middle joint of the finger so that it can actively bend or reroute the cable so that more torque is applied at that joint.

Regarding the cable driving mechanism, some issues still remain. The additional capstan that had to be introduced to compensate for the limited rotation of the servomotor introduced additional friction into the system, which also reduced the grip strength of the finger. This problem can be addressed by replacing the actuator of the finger with a different servomotor with 180 degrees of rotation or installing a separate dc motor and encoder combination. Another possible solution is to replace the encoder with a hall-effect sensor placed inside the finger pads to detect contact between finger and the grasped object. Position sensing for the actuator driving the finger is not necessary for the function of the grasp and was only used as a convenient method for proving the grasp.

B. Compliant Finger Pad

Despite the large error between the experimental results and the simulation results, the finite element model (FEM) of the silicone rubber is promising given the approximations used setup the simulation. For the 10 N load, the finger pad was experiencing strains greater than 100%, at which point the material was no longer behaving linearly. Additionally, the unit cell analysis setup consisted of a 1.0 N load applied to the cell, which would explain the loss in accuracy of the finger pad simulation as the load increases, especially as the strain approaches the hyperelastic region. The source of the 5.7% error is likely due to the method for estimating of the stiffness. The stiffness of the material depended on the directional deformation of the unit

cell. However, applying a 1.0 N load on the unit cell produced a gradient of deformation throughout the surface of the cell. The stiffness was approximated by taking the average of each area of deformation under the assumption that the areas were uniform. Any areas on the surface that were small relative to other deformation areas were neglected. It is possible to export the data so that the deformation at each node can be determined. However, it was impossible to determine the location of each node on the unit cell, therefore eyeballing the areas was the only method available. As a result, the stiffness of the unit cell was a rough approximation where the error propagated into the effective modulus calculations.

The accuracy of the simulation results compared to the experimental results show the feasibility of designing the compliance of finger pads beyond the limitations of material properties. Better methods for estimating the stiffness of the material must be implemented to improve the accuracy of the model. Also, simulations for a range of different applied loads may be necessary to improve the predictions of the FEM.

Regarding the fabrication process of the finger pad, the current method using dissolvable mold needs improvement. The molds were printed out of HIPS plastic printed from the Makerbot Replicator 2x. The molds were then dissolved in d-limonene, a liquid hydrocarbon typically used as a solvent for cleaning solutions. Depending on the geometry of the mold, the lead time for fabricating the finger pad can be upward of one week. During the dissolving process, the silicone rubber will absorb the liquid and expand; the rubber will contract a few days afterward. At the end of the entire process, it was clear that the d-limonene solution affected the properties of the silicone rubber. The finger pad contracted to a size smaller than intended, which resulted in a different geometry than the intended design. An image of the fabrication result is shown in Figure 34.

Figure 34 - Top: finger pad fabricated using dissolvable mold process. The red arrow indicates a region where the rubber is peeling away from the fixtures due to contraction. Bottom: finger pad fabricated using a breakable mold

Figure 34 also displays a separate finger pad, which was fabricated using a mold that was broken off instead of dissolved. This control group produced a finger pad with the desired geometry. However, not all geometries can be achieved through a breakable mold. To make the dissolvable mold process practical, either a different material that doesn't absorb the d-limonene should be used for the finger pad or the d-limonene solution should be substituted for a different solvent. This may also require the mold to be fabricated out of a different material.

C. Locomotion

Evaluation of the locomotion capabilities of the prototype was limited. Without the correct material for the rigid finger, the prototype could not be tested for impact to validate the

FEA optimization. An attempt was made to redesign the finger using a different 3D printed material, however the results of the optimization showed that the size of the finger would have to increase significantly in order to achieve the same durability as the original design. Consequently, the prototype was not ready to be mounted onto the uBot-7 or any other device to evaluate the effectiveness of the manipulator for performing different types of locomotion. In concept, the geometry of the prototype should allow the uBot-7 to perform important locomotion tasks such as knuckle walking, tripedal stance, climbing back from a prone position, etc. Before it can be implemented onto the uBot-7, the prototype should add a rotational degree of freedom to the wrist to improve the range of motion for the finger. This will allow the hand to be oriented in any position to make contact with the ground without relying on the uBot-7's shoulder actuator and upper arm actuator to position the hand, both of which have a limited range of motion. Additional range of motion for the wrist flexion and extension should be added to improve the flexibility of the hand.

The current design also does not have a tensioning mechanism for the drive belt or the cables that connect to the wrist .Consequently there is significant backlash in the system which negatively affects the sensing capabilities of the device. The future prototype should incorporate a belt tensioner and a cable tensioner in order to eliminate backlash.

For the series elastic actuator, the current prototype is able to sense contact with the ground. With an encoder measuring the position of the drive shaft and another encoder to measure the deflection of the spring, closed loop control can be implemented for the prototype to control the position of the wrist. Closed loop control is necessary for the device to ensure that the wrist is moved to the correct position regardless of any disturbances introduced into the system or any passive dynamics from the series spring or friction in the system. For this prototype,

performing system identification first would be necessary before designing a controller. Design of the controller will be reserved for future work, however a framework for a full state feedback controller will be laid out to demonstrate the controllability of the prototype. The parameters of the controller will be tuned empirically as a proof of concept.

VI. Conclusion

The impacts of this type of research are far reaching. From a direct point of view, a hybrid hand foot end effector will increase the functions of a robotic system. A basic humanoid robot with two legs and two hands can now possess four hands and four legs without a significant increase in size or weight. This gives the robot additional methods and strategies for picking up and manipulating objects or moving through free space. Increasing the flexibility of the system improves its performance in unpredictable environments or disaster relief scenarios. Extending to biological applications, a dual function manipulator and locomotion hand can be a suitable replacement for upper limb amputees. Many prosthetic hands designs are focused on improving dexterous manipulation capabilities, but few designs consider the importance of a robust morphology for surviving falls or projectile impacts. Consequently, these prosthetic hands are not suitable for all applications and are generally limited to loads below the limits of the average human hand. Any designs that possess such a level of structural integrity exceed the weight limit for practical use. The research conducted for this honors thesis contributes to future work on more robust prosthetic hands.

Several recommendations can be made for future improvements to the design. Currently the finger has no tactile sensing and is therefore unable to detect when it is gripping an object. Ideally the actuator for the active finger can be switched with a series elastic actuator to provide contact sensing in addition to shock protection. Additionally the wrist is limited to flexion and extension but does not possess any rotation. Given the dimensional requirements of the robotic hand, it is entirely possible to incorporate an additional actuator for wrist rotation. There is also a lot of potential in the design of compliant finger pads by improving the accuracy of FEA predictions and dissolvable molding fabrication process. The current finger pad design is still too

stiff to produce meaningful compliance from the load applied by the active finger. Either the finger should be redesigned for increased compliance under low loads or the actuator driving the finger should be replaced with a higher power motor. These improvements will make the prototype a viable end effector for the uBot-7 and other quadrupedal robots.

Acknowledgements

Special thanks to both Professor Sup and Professor Grosse for giving me the opportunity to work with them and to learn from them. This thesis would not have been possible without their guidance. I would like to express my appreciation to Professor Sup in particular for his advice and help throughout the year. I would not be where I am today without his assistance. I would also like to thank every member of the MRRL for their continuous support along the way. I have not met a group of people more willing to help out another student than the members of this lab and it has been a privilege to work with them. Finally, thanks to Andrew Sciotti for taking the time to edit my thesis during finals week.

References

[1] T. Laliberté and C. M. Gosselin, 'Simulation and design of underactuated mechanical hands', *Mechanism and Machine Theory*, vol. 33, no. 1–2, pp. 39–57, 1998.

[2] J. K. Salisbury and B. Roth, 'Kinematic and Force Analysis of Articulated Mechanical Hands', *Journal of Mechanisms Transmissions and Automation in Design*, vol. 105, no. 1, 1983.

[3] A. Rodriguez, M. T. Mason, and S. Ferry, 'From caging to grasping', *The International Journal of Robotics Research*, vol. 31, no. 7, pp. 886–900, 2012.

[4] Ciocarlie, Matei, Corey Goldfeder, and Peter Allen. 2007. Dimensionality reduction for hand-independent dexterous robotic grasping. Paper presented at IEEE/RSJ International Conference on Intelligent robots and Systems, San Diego, California.

[5] Carrozza, C. M., G. Cappiello, S. Micera, B. B. Edin, L. Beccai, and C. Cipriani. 2006. Design of a cybernetic hand for perception and action. *Biological Cybernetics*.

[6] Jaffar, Ahmed, S. M. Bahari, Cheng Yee Low, and Roseleena Jaafar. Design and control of a multifingered anthropomorphic robotic hand. *International Journal of Mechanical & Mechatronics Engineering* 11 (4): 24-31.

[7] Jung, Sung-Yoon, Sung-Kyun Kang, Myoung-Jun Lee, and Inhyuk Moon. 2007. Design of robotic hand with tendon-driven three fingers. Paper presented at International Conference on control, Automation and Systems, Seoul, Korea.

[8] Zollo, Loredana, Stefano Roccella, Eugenio Guglielmelli, C. M. Carrozza, and Paolo Dario. 2007. Biomechatronic design and control of an anthropomorphic artificial hand for prosthetic and robotic applications. *IEEE/ASME Transactions on Mechatronics* 12 (4): 418-29.

[9] Cabas, Ramiro, Luis M. Cabas, and Carlos Balaguer. 2006. Optimized design of the underactuated robotic hand. Paper presented at IEEE International Conference on Robotics and Automation, Orlando, Florida.

[10] Kurita, Yuichi, Yasuhiro Ono, Atsutoshi Ikeda, and Tsukasa Ogasawara. Human-sized anthropomorphic robot hand with detachable mechanism at the wrist. *Mechanism and Machine Theory* 46: 53-6.

[11] Ueda, Jun, Masahiro Kondo, and Tsukasa Ogasawara. 2012. The multifingered NAIST hand system for robot in-hand manipulation. *Mechanism and Machine Theory* 45: 224-38.

[12] Kim, Eun-Hye, Seok-Won Lee, and Yong-Kwun Lee. 2011. A dexterous robot hand with a bio-mimetic mechanism. *International Journal of Precision Engineering and Manufacturing* 12 (2): 227-35.

[13] Liu, H., K. Wu, P. Meusel, G. Hirzinger, M. H. Jin, Y. W. Liu, S. W. Fan, and Lan, T., Chen, Z.P. 2008. A dexterous humanoid five-fingered robotic hand. Paper presented at 17th IEEE International Symposium on Robot and Human Interactive Communication, Munich, Germany.

[14] Yamaguchi, Akihiro, Kenjiro Takemura, Shinichi Yokota, and Kazuya Edamura. 2011. A robot hand using electro-conjugate fluid. *Sensors and Actuators A*: 139-46.

[15] Takaki, Takeshi, and Toru Omata. 2011. High-performance anthropomorphic robot hand with grasping-force-magnification mechanism. *IEEE/ASME Transactions on Mechatronics* 16 (3): 583-91.

[16] R. R. Ma, A. Spiers, and A. M. Dollar, 'M2 Gripper: Extending the Dexterity of a Simple, Underactuated Gripper.'

[17] S. Kang, H. In, and K. Cho, "Design of a passive brake mechanism for tendon driven devices," *International Journal of Precision Engineering and Manufacturing*, vol. 13, no. 8, pp. 1487–1490, 2012.

Appendix A – Rigid Finger Optimization Process

1) Explicit Dynamics Setup: 30 kg weight applied to top of finger. Insert standard earth gravity

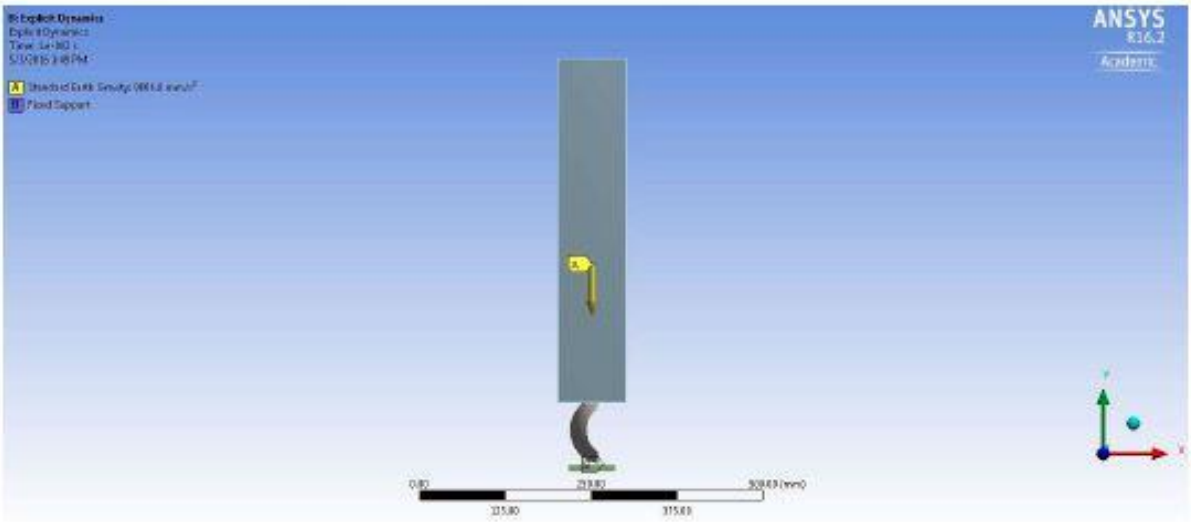

To reduce solve time, the volume of the weight was increased. The run time for explicit dynamics solver is a function of both model size and time step. In explicit dynamics, the time step is calculated internally to ensure a stable solution. This is to ensure that the stress wave does not travel more than the smallest element size in a single time step. This condition is known as the Courant condition given below,

$$\Delta t \leq f * \left[\frac{h}{c}\right]_{\min}$$

t - time step
f - scale factor to improve stability
h - smallest element dimension in model
c - stress wave speed

the stress wave speed can vary for different elements, but a rough estimation is given by,

$$c = \sqrt{\frac{E}{\rho}}$$

c - stress wave speed
E - Young's modulus
p - density

Given the Courant condition, increasing the density will decrease the stress wave speed, which will consequently increase the time step.

$V_{weight} := 60\ mm \cdot 100\ mm \cdot 500\ mm = 0.003\ m^3$ volume of weight

$mass := 30\ kg$ target mass

$\rho := \frac{mass}{V_{weight}} = \left(1 \cdot 10^4\right) \frac{kg}{m^3}$ density of weight

Solve time is further reduced by positioning the object closer to the ground and adding an initial velocity to the setup. The finger is positioned 50mm from the ground.

$h_i := .5 \cdot m$ $h_{setup} := .5\ mm$

$energy_{total} := mass \cdot g \cdot h_i = 147.1\ J$

$energy = .5 \cdot m \cdot V^2$

$V = \sqrt{\frac{2 \cdot energy}{m}}$

$V_i := \sqrt{\frac{2 \cdot \left(energy_{total} - mass \cdot g \cdot h_{setup}\right)}{mass}} = \left(3.13 \cdot 10^3\right) \frac{mm}{s}$

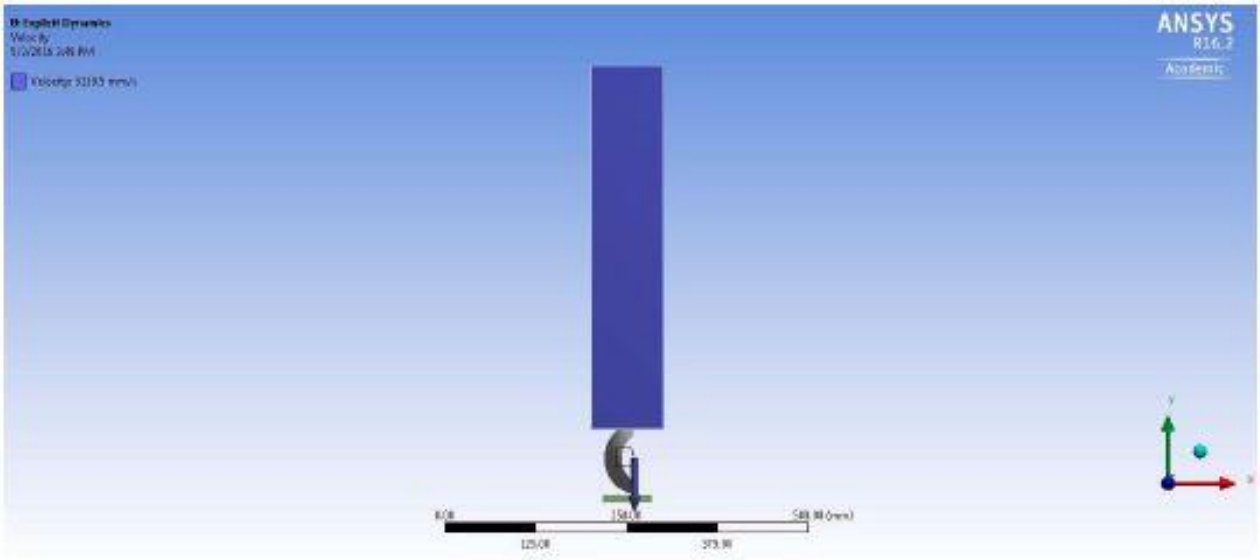

Finally, the mesh is also set to coarse to improve the solve time even further. The optimization results are validated again with a finer mesh at the end.

Mesh: 660 nodes, 2125 elements

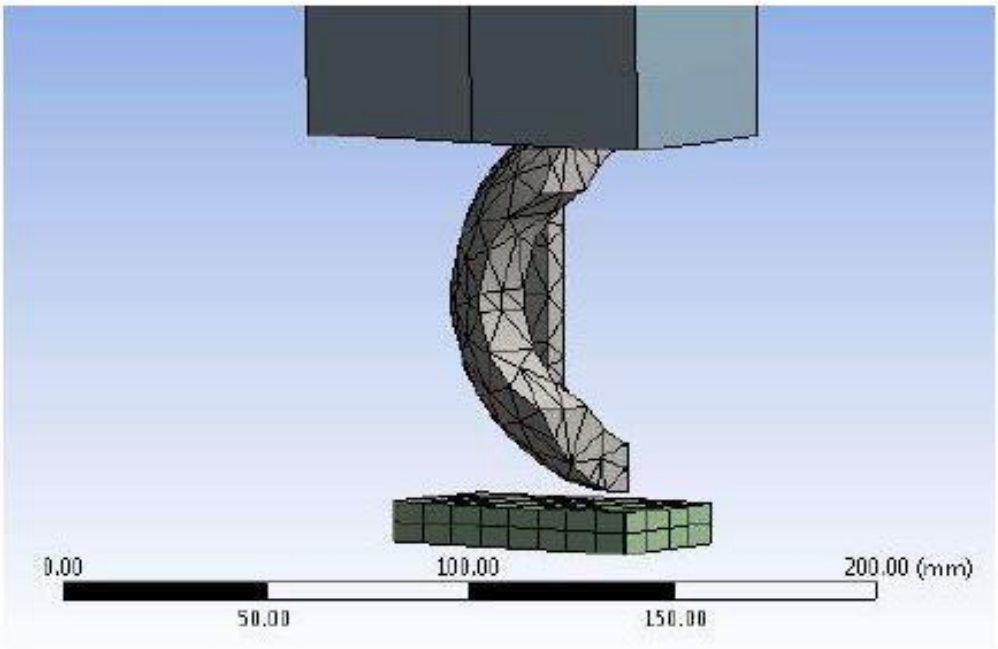

A design of experiments was setup with solid mass and safety factor as outputs, and design parameters of the finger as inputs. A curve is then fit to the outputs of the design of experiments. The accuracy of the curve fit is displayed below.

Table of Schematic D3: Response Surface

	A	B	C
1		P9 - Solid Mass	P14 - Safety Factor Minimum Minimum Value Over Time
2	Coefficient of Determination (Best Value = 1)		
3	Learning Points	0.99525	0.77611
4	Root Mean Square Error (Best Value = 0)		
5	Learning Points	0.0011404	0.00076234
6	Relative Maximum Absolute Error (Best Value = 0%)		
7	Learning Points	10.891	75.28
8	Relative Average Absolute Error (Best Value = 0%)		
9	Learning Points	5.498	39.776

Note that the curve does not fit the design of experiment points accurately, especially in regards to safety factor. The optimization method is later switched to direct optimization.

Below displays the sensitivity of the solid mass and safety factor to the design parameters.

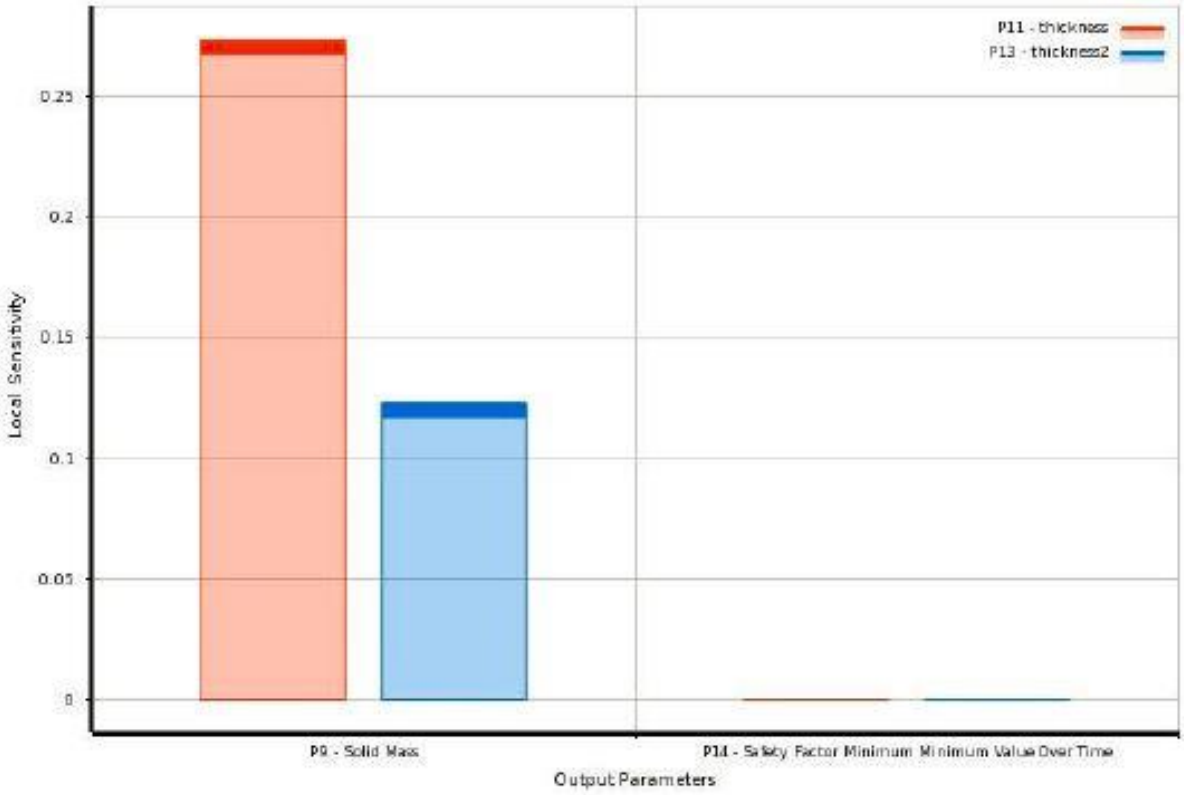

The local minima on the response curve represent different optimal rigid finger designs. The NLPQL (Nonlinear Programming by Quadratic Lagrangian) search algorithm is used to find local minima. This was repreated multiple times until the candidate with the lowest mass is produced. Results are displayed below.

Table of Schematic E4: Optimization

	A	B	C	D	E	F	G	H
1	Optimization Study							
2	Minimize P9	Goal, Minimize P9 (Default importance)						
3	P14 >= 1	Strict Constraint, P14 values greater than or equals to 1 (Default importance)						
4	Optimization Method							
5	NLPQL	The NLPQL method (Nonlinear Programming by Quadratic Lagrangian) is a gradient-based algorithm to provide a refined, local, optimization result. It supports a single output parameter objective, multiple constraints and is limited to continuous parameters. The starting point must be specified to determine the region of the design space to explore.						
6	Configuration	Approximate derivatives by Central difference and find 3 candidates in a maximum of 20 iterations.						
7	Status	Converged after 13 evaluations.						
8	Candidate Points							
9		Starting Point	Starting Point (verified)	Candidate Point 1	Candidate Point 1 (verified)	Candidate Point 2	Candidate Point 3	Candidate Point 3 (verified)
10	P11 - thickness (mm)	15		10		12.323	15	
11	P13 - thickness2 (mm)	5.5		1		3.9034	5.5	
12	P9 - Solid Mass (lbm)	0.14473	0.14282	0.1072	0.10713	0.12806	0.14473	0.14282
13	P14 - Safety Factor Minimum Minimum Value Over Time	1.001	1.0007	1.0018	1.0015	1.0013	1.001	1.0007

Candidate point 1 is selected to be the optimal finger design. The design is verified in ANSYS with a finer mesh.

Mesh: 2862 Nodes, 3606 Elements

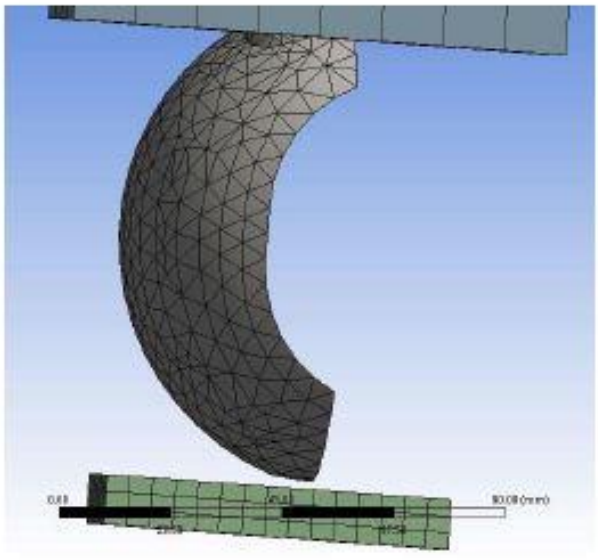

Results of the analysis are displayed below.

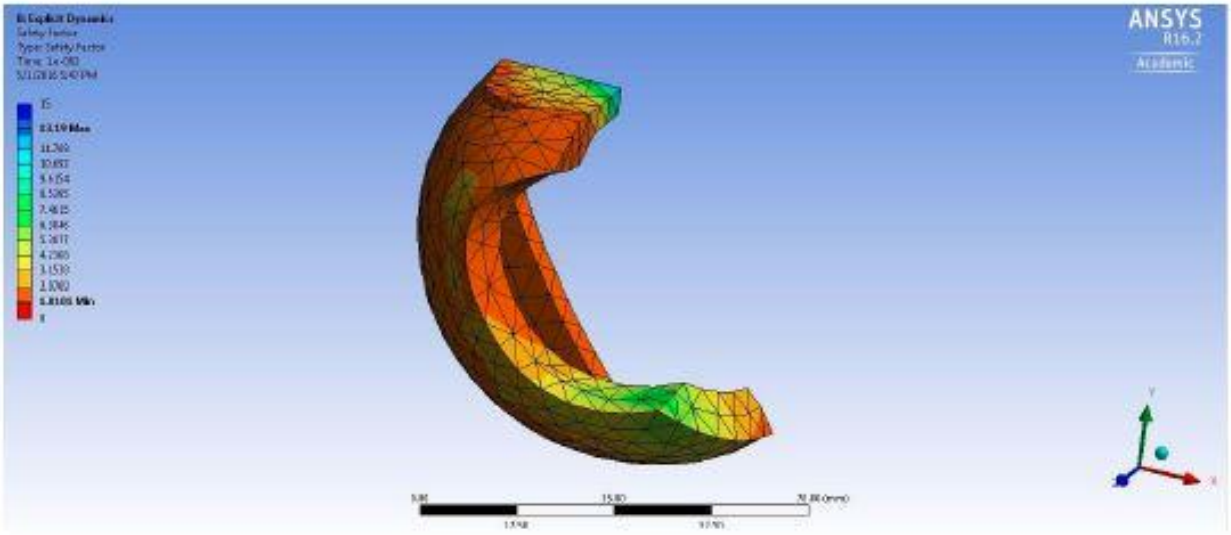

Not that the safety factor is close to the predicted valuesf rom the response curve. This may not always be the case given the curve's poor goodness of fit

Appendix B – Finite Element Analysis on Plate Components

Static Structural Analysis: All plates are made of PA2200 Performance 1.0. A 30 kg load static is applied in compression. The target safety factor is 3 to compensate for any dynamic loads. Explicit dynamics was not used because there was no method to determine the distribution of energy throughout the system under impact conditions. All anlaysis has a 5% convergence criterion.

Setup for Plates 1 and 2

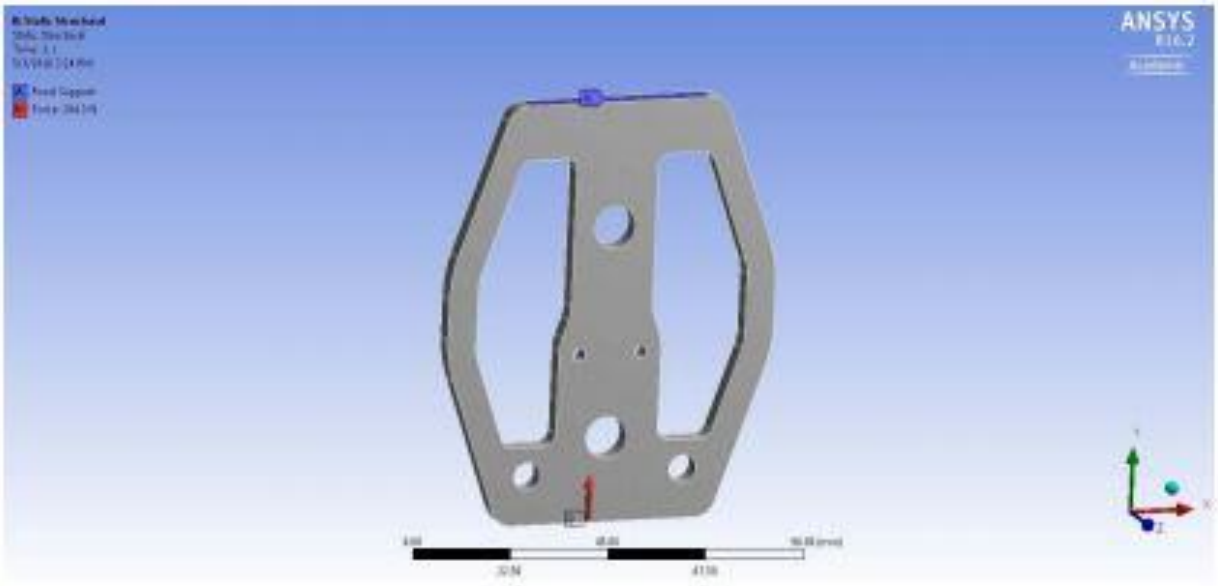

Setup for Plates 3

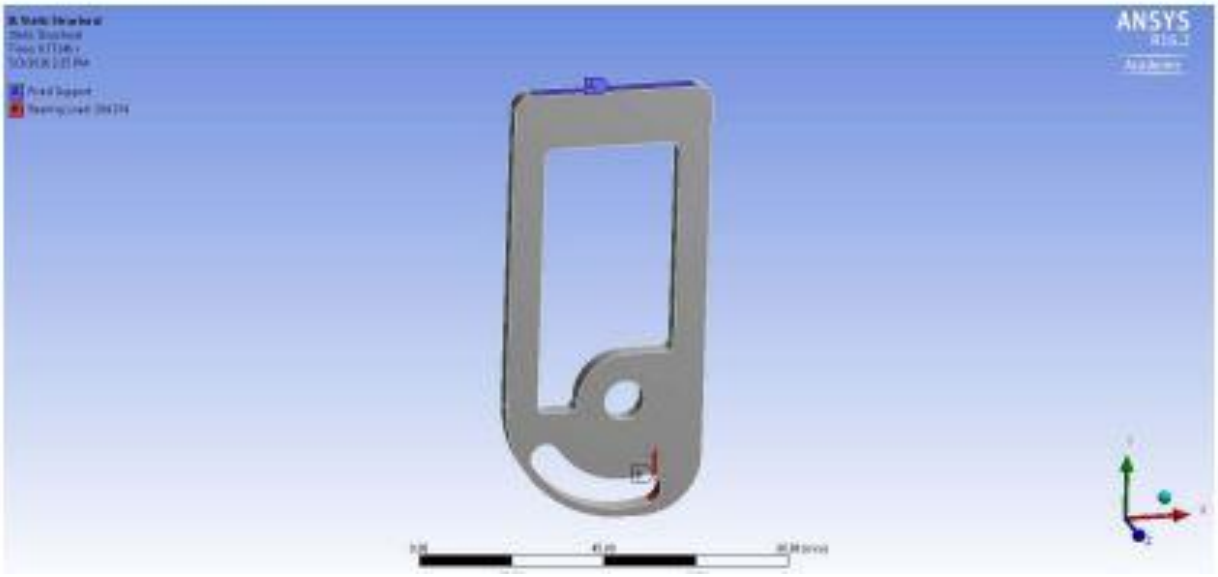

Plate 1 Results: Safety Factor = 4.87

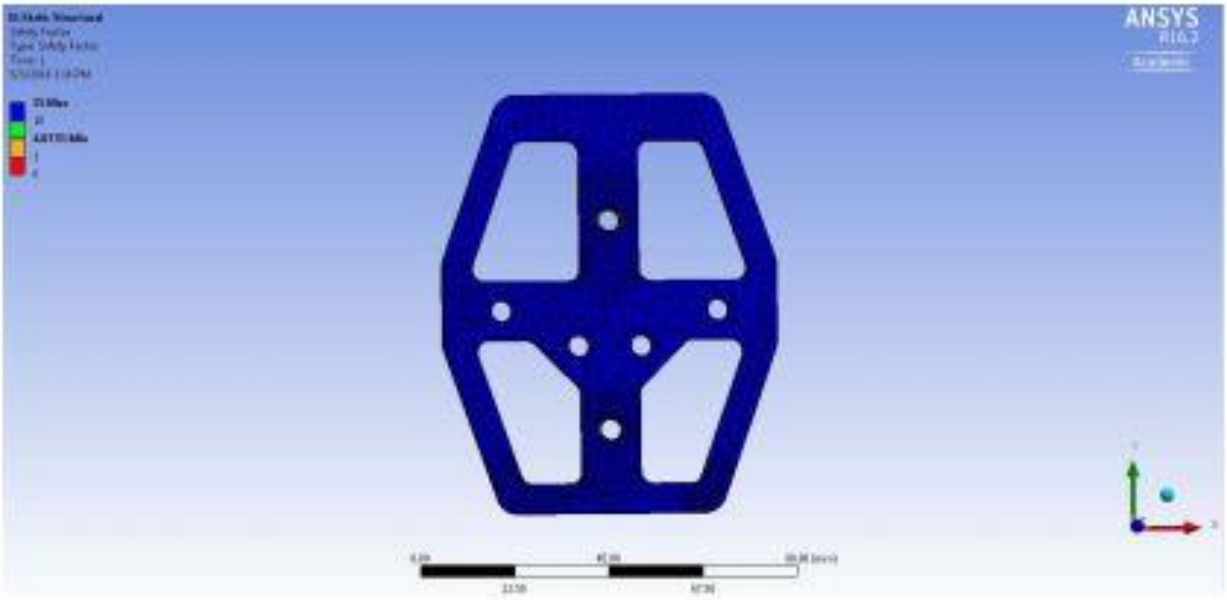

Plate 2 Results: Safety Factor = 4.35

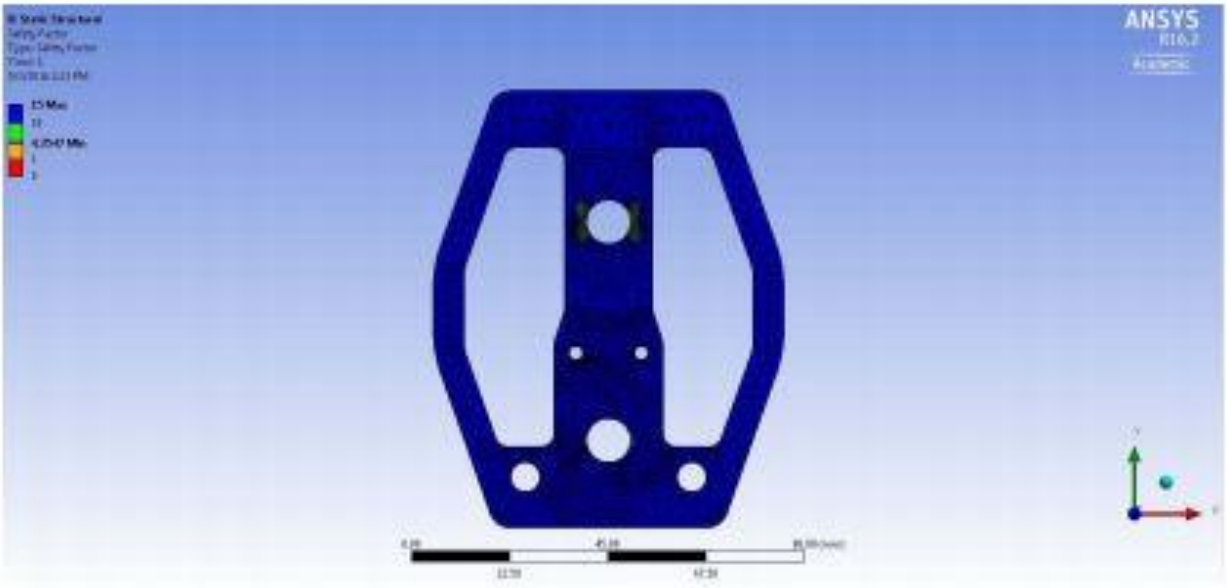

Plate 2 Results: Safety Factor = 3.56

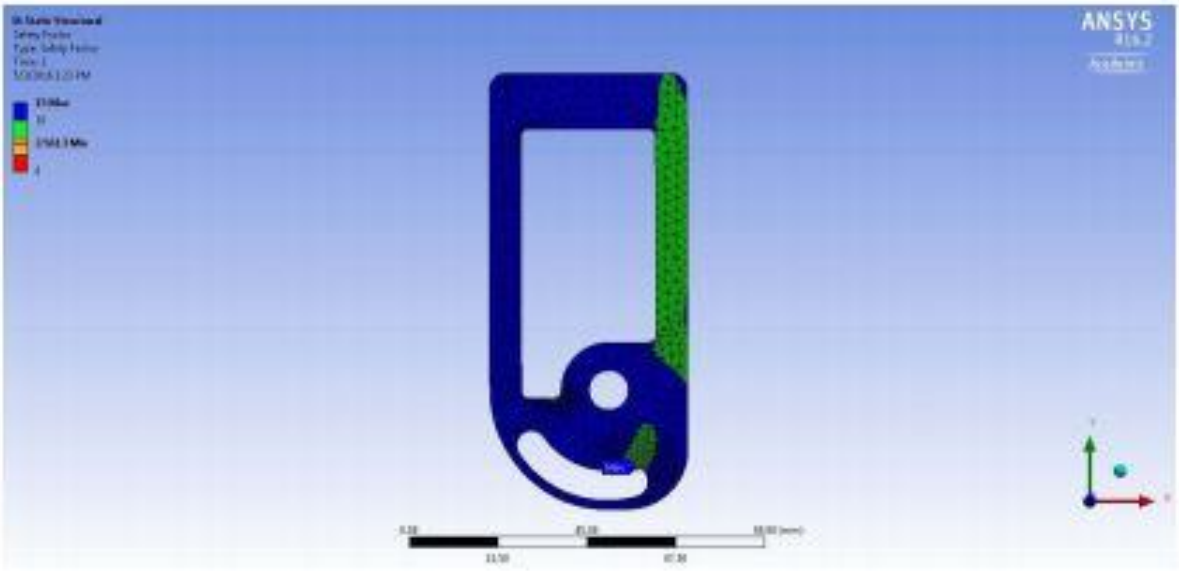

Note: high safety factors in all three plates show that the designs can be optimized. Optimization was attempted, but the results produced unrealistic dimensions for each part. Additionally, the weight that is saved from optimizing the design is negligible compared to the mass of the prototype. The final weight of the prototype is also within the acceptable range.

Appendix C – Tabulated Data from Unit Cell Analysis

Radius (mm)	Force (N)	Deformation (directional, mm)	Effective Moduluse (Pa)	Deformation (mm)	%error	Modulus (4th order approximation)	%error
0.5	1	0.18772	247200	0.189525	-0.96	247226.375	-0.01
1	1	0.2199	215000	0.21791	0.90	214872	0.06
1.5	1	0.270295	175000	0.26772	0.95	175259.625	-0.15
2	1	0.36544	128000	0.366015	-0.15	127745	0.20
2.5	1	0.600998571	78000	0.600645	0.05	78133.875	-0.17
3	1	1.21282625	38700	1.2106	0.18	38682	0.05

Appendix D – Mobility Equation for Finger Actuation

Kreubler's Criterion for Mobility

$$M = 3 \cdot (N-1) - 2 \cdot f_1 - f_2$$

M - number of degrees of freedom in the system
N - number of links in the system
f1 - number of links with 1 degree of freedom
f2 - number of links with 2 degrees of freedom

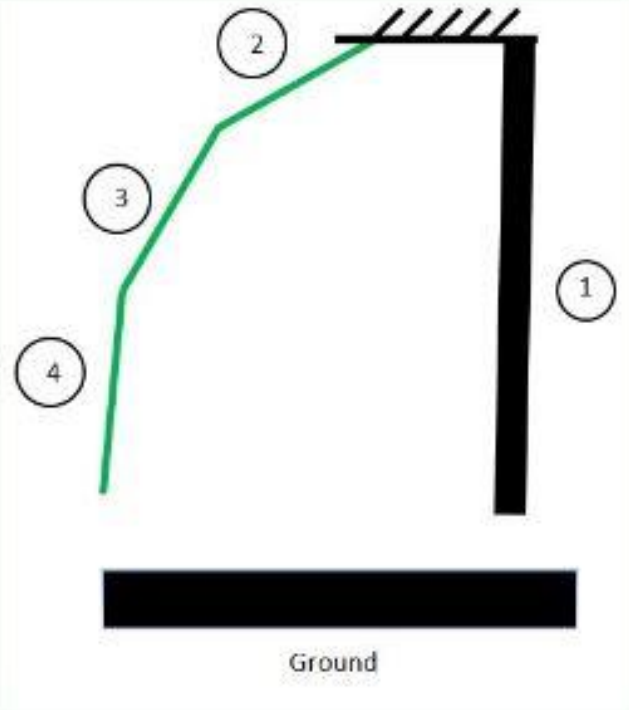

$N := 4$
$f_1 := 4$
$f_2 := 0$

$M := 3 \cdot (N-1) - 2 \cdot f_1 - f_2 = 1$

1 degrees of freedom in this system for picking up objects from a flat surface

Appendix E – Motor Selection

Wrist Actuator

$W_{max} := 16\ oz \cdot g = 1\ lbf$ Maximum load on the finger

$C := 2$ correction factor due to friction/other losses

$R := \frac{10}{15}$ reduction ratio

$L_{finger} := 80\ mm$ approximate distance between load and wrist joint

$W_{base} := 50\ mm$ approximate horizontal distance from wrist joint to spring

$r_{pulley} := 10\ mm$ approximate radius of pulley attached to the motor

$w_{motor} := \frac{W_{base} \cdot 90\ \frac{deg}{s}}{r_{pulley}} = 75\ rpm$ minimum rotational speed of shaft to achieve 90 deg/s rotation of the wrist

$p_{motor} := W_{max} \cdot C \cdot L_{finger} \cdot w_{motor} = 5.59\ W$

$\tau_{motor} := W_{max} \cdot L_{finger} \cdot \frac{10}{15} = 0.237\ N \cdot m$ required torque from the motor

Motor: Maxon EC 32 Flat, brushless, 6W
Gearhead: Maxon GP 22 A Metal Version

$K_t := 9.5 \cdot 10^{-3} \cdot \frac{N \cdot m}{A}$ torque constant

$i := .913 \cdot A$ nominal current (max continuous current)

$\tau_{Maxon} := K_t \cdot i = 0.009\ N \cdot m$ maximum continuous output torque

$R := 29$ reduction ratio

$\tau_{cont} := R \cdot \tau_{Maxon} = 0.252\ N \cdot m$ $\tau_{cont} > \tau_{motor} = 1$ True

Finger Actuator

$F_{cable} := 6\ lbf$ minimum tension in cable required gripping 1 lbf object

$w_{motor2} := 90\ \frac{deg}{s}$ minimum speed of motor

$r_{pulley} := 10\ mm$ radius of pulley

$P_{motor} := F_{cable} \cdot r_{pulley} \cdot w_{motor2} \cdot C = 0.838\ W$

$\tau_{motor2} := F_{cable} \cdot r_{pulley} = 0.267\ N \cdot m$

Motor: Hitec HS-5645mg

Specifications

Motor Type:	3 Pole
Bearing Type:	Dual Ball Bearing
Speed (4.8V/6.0V):	0.23 / 0.18
Torque oz./in. (4.8V/6.0V):	143 / 168
Torque kg./cm. (4.8V/6.0V):	10.3 / 12.1
Size in Inches:	1.59 x 0.77 x 1.48
Size in Millimeters:	40.39 x 19.56 x 37.59
Weight ounces:	2.11
Weight grams:	59.82

$\tau_{hitec} := 168 \cdot ozf \cdot in$

$\tau_{hitec} > \tau_{motor2} = 1$ True

$\omega_{hitec} := \frac{60\ deg}{.18} \cdot \frac{1}{s} = 55.556\ rpm$

$\omega_{hitec} > w_{motor2} = 1$ True

Appendix F – Spring Selection

Case: Falling from upright position with arms at 90 degrees

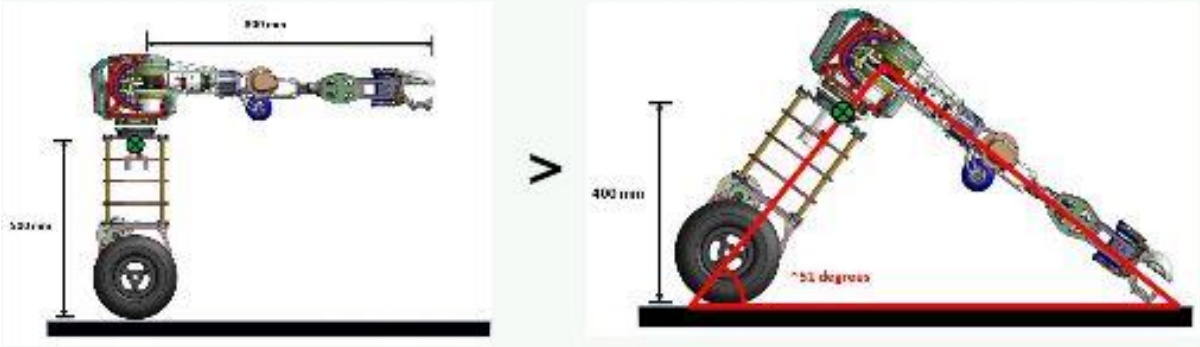

Assumptions: uBot-7 falls one hand. All of the energy is absorbed by the spring. This is an overestimated scenario because the impact energy will be distributed throughout the hand. As a result, the factor of safety is implied.

$h := .11 \cdot m$ — vertical distance different between upright position to fall position (center of mass)

Assumption: arms are parrallel to ground, wheels are on the ground

$E_{gear} := 30 \cdot J$ — Approximate fracture toughness of steel for impact

$m := 30\ kg$ — mass of ubot-7

$E_{max} := \left(m \cdot g \cdot h - E_{gear}\right) = 2.362\ J$ — energy springs must absorb to protect motor

Spring: Century Spring #80713

$x := .76 \cdot in$ — rated deflection of spring

$N := 3$ — number of springs in parallel

Extension Spring 80713

Part Characteristics

CSC Stock #	80713
OD (in)	0.5000
Length (in)	1.5000
Rate (lbs/in)	26.0000
Initial Tension (lbs)	2.0000
Sugg. Max. Defl. (in)	0.7692
Sugg. Max. Load (lbs)	21.0000
Wire Dia. (in)	0.0630
Material	Music Wire
Finish	None

$k := \frac{E_{max} \cdot 2}{N \cdot x^2} = 24.129\ \frac{lbf}{in}$

Spring Deflection Under Static Load

$k_{eq} := N \cdot k = 72.386 \ \frac{lbf}{in}$ equivalent spring constant

$L_{finger} := 80 \ mm$ approximate distance between load and wrist joint

$W_{base} := 50 \ mm$ approximate horizontal distance from wrist joint to spring

$res := 2048$ resolution of encoder

$\theta_{min} := \frac{360 \ deg}{res} = 0.176 \ deg$ minimum angle measured by encoder

$\theta_{allowable} := \theta_{min} \cdot 20 = 3.516 \ deg$ minimum allowable angle that wrist must deflect to be detected by the encoder

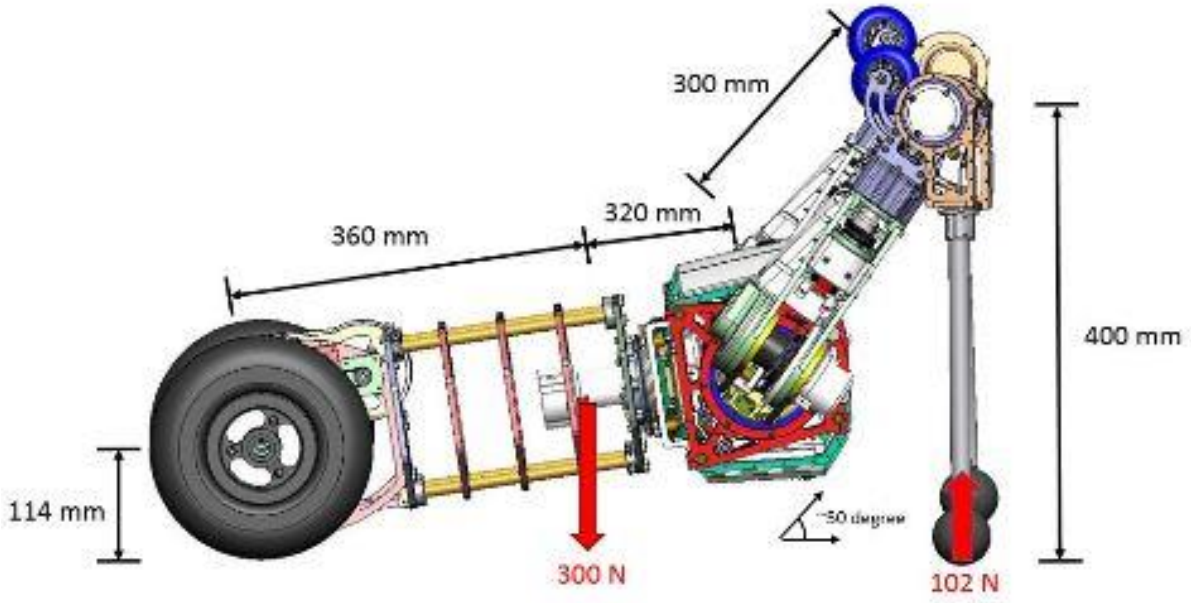

The dimensions in the figure above are used in the calculations for the spring deflection under different loading conditions.

Prone Position

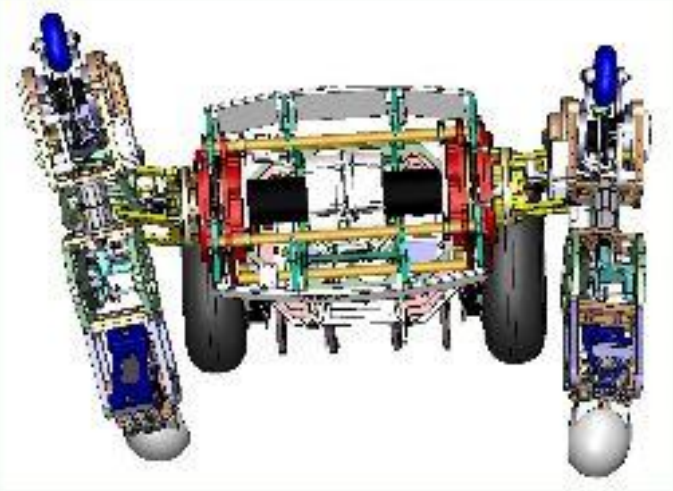

$$d_{prone} := \frac{m \cdot g \cdot \frac{360\ mm}{(360+320+300 \cdot \sin(50\ deg))\ mm} \cdot \frac{L_{finger}}{W_{base}}}{k_{eq}} = 14.693\ mm$$

minimum deflection in spring

$$\theta_{prone} := \operatorname{atan}\left(\frac{d_{prone}}{W_{base}}\right) = 16.376\ deg$$

wrist angle: prone position

$$\theta_{prone} > \theta_{allowable} = 1$$

true

Tripedal Stance

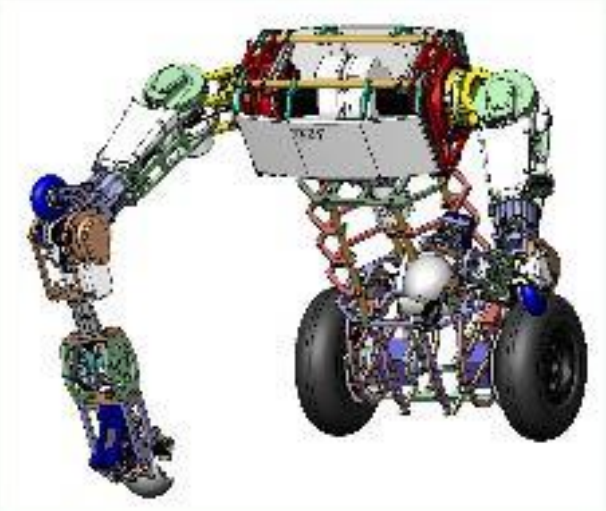

assumption, weight of uBot is distributed evenly among 3 members: 2 wheels and 1 hand

$$d_{tri} := \frac{m \cdot g \cdot \frac{1}{3} \cdot \frac{L_{finger}}{W_{base}}}{k_{eq}} = 12.378\ mm$$

$$\theta_{tri} := \operatorname{atan}\left(\frac{d_{tri}}{W_{base}}\right) = 13.904\ deg$$

$$\theta_{tri} > \theta_{allowable} = 1$$

true

Appendix G – Prototype Weight Calculation

$\rho_{PA2200} := 930 \cdot \frac{kg}{m^3}$ $\rho_{silicone} := \frac{1}{25} \cdot \frac{lbm}{in^3}$ $\rho_{steel} := .289 \frac{lbm}{in^3}$ $\rho_{al} := 2700 \frac{kg}{m^3}$

$V_{plate1} := 14553 \cdot mm^3$ $V_{silicone} := 13714\ mm^3$

$V_{plate2} := 20429\ mm^3$

$V_{plate3} := 20570\ mm^3$

$V_{base} := 82553\ mm^3$

$V_{finger\_appendage} := 6592\ mm^3$

$V_{output\_link} := 11711\ mm^3$

$V_{rigid\_finger} := 20267\ mm^3$

$V_{m\_housing} := 29680\ mm^3$

$m_{silicone} := \rho_{silicone} \cdot V_{silicone} = 0.015\ kg$

$m_{hand} := \rho_{PA2200} \cdot \left(3 \cdot V_{finger\_appendage} + V_{base} + V_{rigid\_finger}\right) = 0.114\ kg$

$m_{wrist} := \rho_{PA2200} \cdot \left(2 \cdot V_{plate1} + V_{plate2} + V_{plate3} + 3 \cdot V_{output\_link} + V_{m\_housing}\right) = 0.125\ kg$

$m_{misc} := \rho_{PA2200} \cdot 65700\ mm^3 = 0.061\ kg$

$m_{motor} := 32\ gm$

$m_{gearhead} := 55\ gm$

$m_{servo} := 60\ gm$

$m_{steel} := \rho_{steel} \cdot 9364\ mm^3 = 0.075\ kg$

$m_{al} := \rho_{al} \cdot 26737\ mm^3 = 0.072\ kg$

$m_{total} := m_{silicone} + m_{hand} + m_{wrist} + m_{misc} + m_{motor} + m_{gearhead} + m_{servo} + m_{steel} + m_{al}$

$m_{total} = 0.61\ kg$